




ARTICLE

A *DNAH17* missense variant causes flagella destabilization and asthenozoospermia

Beibei Zhang^{1*}, Hui Ma^{1*}, Teka Khan^{1*}, Ao Ma¹, Tao Li¹, Huan Zhang¹, Jianing Gao¹, Jianteng Zhou¹, Yang Li¹, Changping Yu¹, Jianqiang Bao¹ , Asim Ali¹ , Ghulam Murtaza¹, Hao Yin¹, Qian Gao¹, Xiaohua Jiang¹, Feng Zhang^{2,3,4}, Chunyu Liu², Ihsan Khan¹, Muhammad Zubair¹, Hafiz Muhammad Jafar Hussain¹, Ranjha Khan¹, Ayesha Yousaf¹, Limin Yuan⁵, Yan Lu⁵, Xiaoling Xu⁶, Yun Wang⁶, Qizhao Tao¹, Qiaomei Hao¹, Hui Fang¹, Hongtao Cheng¹, Yuanwei Zhang¹, and Qinghua Shi¹ 

Asthenozoospermia is a common cause of male infertility, but its etiology remains incompletely understood. We recruited three Pakistani infertile brothers, born to first-cousin parents, displaying idiopathic asthenozoospermia but no ciliary-related symptoms. Whole-exome sequencing identified a missense variant (c.G5408A, p.C1803Y) in *DNAH17*, a functionally uncharacterized gene, recessively cosegregating with asthenozoospermia in the family. *DNAH17*, specifically expressed in testes, was localized to sperm flagella, and the mutation did not alter its localization. However, spermatozoa of all three patients showed higher frequencies of microtubule doublet(s) 4–7 missing at principal piece and end piece than in controls. Mice carrying a homozygous mutation (*Dnah17^{M/M}*) equivalent to that in patients recapitulated the defects in patients' sperm tails. Further examinations revealed that the doublets 4–7 were destabilized largely due to the storage of sperm in epididymis. Altogether, we first report that a homozygous *DNAH17* missense variant specifically induces doublets 4–7 destabilization and consequently causes asthenozoospermia, providing a novel marker for genetic counseling and diagnosis of male infertility.

Introduction

According to the World Health Organization (WHO), men whose ejaculates have <32% progressively motile sperm are diagnosed with asthenozoospermia (WHO, 2010). Asthenozoospermia is one of the major causes of male infertility. Isolated asthenozoospermia accounts for 19% of all infertile men, and oligo- and/or terato-asthenozoospermia could account for 63% of all infertile men (Curi et al., 2003). Numerous factors, like lifestyle, pollutants, prolonged sexual abstinence, partial blockage of seminal tract, varicocele, and infection, have been reported as causes of asthenozoospermia (Adams et al., 2014; Ortega et al., 2011; Salas-Huetos et al., 2017). Nonetheless, the genetic factors underlying asthenozoospermia remain largely unknown.

Axoneme is the core structure of sperm flagellum, presenting throughout the flagellar length. The axoneme is typically composed of 9+2 microtubules, where a central pair of microtubules is surrounded by nine peripheral microtubule doublets (MTDs)

in the fixed order (Inaba, 2011). Axonemal dyneins are a pair of projecting “hooks,” consisting of an inner and an outer dynein arm (IDA and ODA, respectively), which are attached to each of the nine MTDs (Kikkawa, 2013). IDAs and ODAs are structural subunits of axoneme and essential for generating beating forces of sperm flagella (Gibbons, 1963; Summers and Gibbons, 1971). Each dynein arm is composed of several light chain proteins, at least two intermediate chain proteins, and at least two heavy chain proteins that hydrolyze ATPs for microtubule sliding (Inaba, 2011; Roberts et al., 2013).

Heavy chains, also known as dynein axonemal heavy chains (DNAHs), comprise 13 members (DNAH1–3, 5–12, 14, and 17) in humans (Pazour et al., 2006). Disruptions in DNAHs, such as *DNAH5* (Hornef et al., 2006; Olbrich et al., 2002), *DNAH6* (Li et al., 2016), *DNAH9* (Fassad et al., 2018; Loges et al., 2018), and *DNAH11* (Bartoloni et al., 2002; Knowles et al., 2012; Lucas

¹The First Affiliated Hospital of University of Science and Technology of China, Hefei National Laboratory for Physical Sciences at Microscale, University of Science and Technology of China-Shenyang Jinghua Hospital Joint Center for Human Reproduction and Genetics, Chinese Academy of Sciences (CAS) Key Laboratory of Innate Immunity and Chronic Diseases, School of Life Sciences, CAS Center for Excellence in Molecular Cell Science, Collaborative Innovation Center of Genetics and Development, University of Science and Technology of China, Hefei, China; ²Obstetrics and Gynecology Hospital, State Key Laboratory of Genetic Engineering at School of Life Sciences, Institute of Reproduction and Development, Fudan University, Shanghai, China; ³Key Laboratory of Reproduction Regulation of National Population and Family Planning Commission, Collaborative Innovation Center of Genetics and Development, Fudan University, Shanghai, China; ⁴Shanghai Key Laboratory of Female Reproductive Endocrine Related Diseases, Shanghai, China; ⁵Analysis and test center, Co-Innovation Center for Modern Production Technology of Grain Crops, Yangzhou University, Yangzhou, China; ⁶Department of Respiration, The First Affiliated Hospital of University of Science and Technology of China, Division of Life Sciences and Medicine, University of Science and Technology of China, Hefei, China.

*B. Zhang, H. Ma, and T. Khan contributed equally to this paper; Correspondence to Qinghua Shi: qshi@ustc.edu.cn; Yuanwei Zhang: zyuanwei@ustc.edu.cn; Hui Ma: clsmh@ustc.edu.cn.

© 2019 Zhang et al. This article is available under a Creative Commons License (Attribution 4.0 International, as described at <https://creativecommons.org/licenses/by/4.0/>).

et al., 2012; Schwabe et al., 2008), are known to cause, or are associated with, primary ciliary dyskinesia (PCD), a genetically heterogeneous disorder that is characterized by chronic airway diseases, left-right laterality disturbances, and male infertility (Leigh et al., 2009). So far, mutations in only *DNAH1* or *DNAH9* have been described in patients with asthenozoospermia. Patients harboring biallelic *DNAH1* mutations were infertile and displayed impaired sperm motility and multiple morphological abnormalities of sperm flagella (MMAF), including absent, bent, short, coiled, and irregular-caliber flagella (Coutton et al., 2018; Ben Khelifa et al., 2014; Sha et al., 2017; Tang et al., 2017; Wang et al., 2017); an infertile patient with two homozygous *DNAH9* mutations displayed markedly reduced sperm counts and motility, as well as absence of morphologically normal sperm (i.e., oligoasthenozoospermia; Fassad et al., 2018), whereas their functional roles in maintaining sperm motility and flagellar structure have not been fully understood. Interestingly, *DNAH17*, encoding an ODA component, showed testis-specific mRNA expression in humans (Milisav and Affara, 1998) but has not yet been functionally characterized.

In this study, we recruited three primary infertile patients from Pakistan, born to a consanguineous union and suffering from asthenozoospermia with no MMAF-like phenotype or ciliary-related symptoms. Through whole-exome sequencing (WES) and Sanger sequencing, we identified a homozygous missense variant in *DNAH17* recessively cosegregating with asthenozoospermia in this family. Further analyses of spermatozoa from patients and functional studies in mice carrying a *Dnah17* mutation equivalent to that in patients collectively demonstrated that the *DNAH17* variant specifically induces doublets 4–7 destabilization during sperm storage in epididymides and thus causes asthenozoospermia, signifying that *DNAH17* is the first DNAH protein implicated in stabilizing flagellar structure.

Results

Three asthenozoospermic patients born to a consanguineous union

This study was performed on a family with male infertility originating from Pakistan (Fig. 1 A). The parents (III:1 and III:2) were first-degree cousins and gave birth to three daughters and four sons. Two sisters (IV:5, 42 yr old and IV:6, 27 yr old) had three and two children, respectively, and the youngest sister (IV:7, 25 yr old), who had normal menstrual cycles, was unmarried. Among the four brothers, one (IV:4, 28 yr old) was unmarried; the other three, IV:1 (43 yr old), IV:2 (41 yr old), and IV:3 (29 yr old), had been married for 20, 17, and 11 yrs, respectively, but all were infertile. They did not have any history of drinking, smoking, exposure to toxic chemicals, or any symptoms of ciliary-related diseases and were physically normal with respect to height, weight, external genitalia, and testicular size. Semen analyses of patients revealed that semen volumes, sperm concentrations, and percentages of morphologically normal sperm fell within the normal ranges (WHO, 2010). However, all three patients exhibited reduced sperm motility, with $\leq 25.0\%$ of motile sperm and $\leq 17.5\%$ progressively motile

sperm. Hence, they were diagnosed with asthenozoospermia. Patients' clinical characteristics are summarized in Table 1.

Identification of a candidate pathogenic variant in *DNAH17*

To understand the genetic cause of asthenozoospermia in this family, we performed WES for patient IV:2 and his father. Following a pipeline of WES data analysis (Fig. S1), 12 variants in 12 genes were retained. Subsequent Sanger sequencing on genomic DNA from all the available family members (III:1, III:2, and IV:1–7) verified four variants in four genes (*DNAH17*, *GPS1*, *HIDI*, and *USP36*) recessively coinherited with asthenozoospermia (Fig. 1 B and Fig. S1 B). *GPS1*, *HIDI*, and *USP36* are annotated ubiquitously expressed in various tissues (Zhang et al., 2013; *DNAH17* mRNA exhibits testis-specific expression [Milisav and Affara, 1998]). Given that our patients did not show any other symptoms except asthenozoospermia, the homozygous missense variant (c.G5408A) in *DNAH17* was favorably presumed to be responsible for the diminished sperm motility in the patients.

The *DNAH17* c.G5408A occurred in exon 35 and caused a G-to-A substitution at cDNA (NCBI reference sequence no. NM_173628) nucleotide position 5408, predicted to replace cysteine (C) by tyrosine (Y) at amino acid position 1803 (p.C1803Y; Fig. 1 C). The altered amino acid is located in the N-terminal stem region of *DNAH17*, which is known to interact with other dynein components. Phylogenetic analysis revealed that the altered amino acid was conserved from lower to higher organisms (Fig. 1 D). All these findings suggest that the homozygous *DNAH17* variant (c.G5408A) could be pathogenic for asthenozoospermia in this family.

Generation and validation of the anti-*DNAH17* antibody

To determine the expression and localization of *DNAH17*, we generated an antibody recognizing an epitope of *DNAH17* amino acids 3502–3801, which is highly conserved between mouse and human (Fig. S2). To test the specificity of this antibody, immunoblotting and immunofluorescence (IF) staining assays were performed with HEK293T cells overexpressing FLAG-tagged epitope-corresponding peptides from mouse and human *DNAH17*, *DNAH9*, and *DNAH11*, which are the mammalian homologues of *Chlamydomonas reinhardtii* ODA β -HCs (Pazour et al., 2006) and have high amino acid sequence similarity. The anti-*DNAH17* antibody showed high affinity to the epitope-corresponding peptides of both mouse and human *DNAH17* as expected. However, it also recognized the overexpressed epitope-corresponding peptides of mouse and human *DNAH9*, as well as mouse *DNAH11*, in immunoblotting assays (Fig. S3 A), and mouse and human *DNAH9* and *DNAH11* in IF staining (Fig. S3 B). To determine whether this anti-*DNAH17* antibody recognizes the endogenous *DNAH9* and *DNAH11* full-length proteins in humans and mice, we performed IF staining of respiratory cilia where *DNAH9* and *DNAH11* have been reported to be expressed (Dougherty et al., 2016; Fliegauf et al., 2005). This anti-*DNAH17* antibody yielded weak signals that were not distinguishable from those of rabbit control IgG (Fig. 2, A and B), indicating that *DNAH17* is not expressed in respiratory cilia, and that this anti-*DNAH17* antibody is not likely to recognize endogenous *DNAH9* and *DNAH11* in humans and mice.

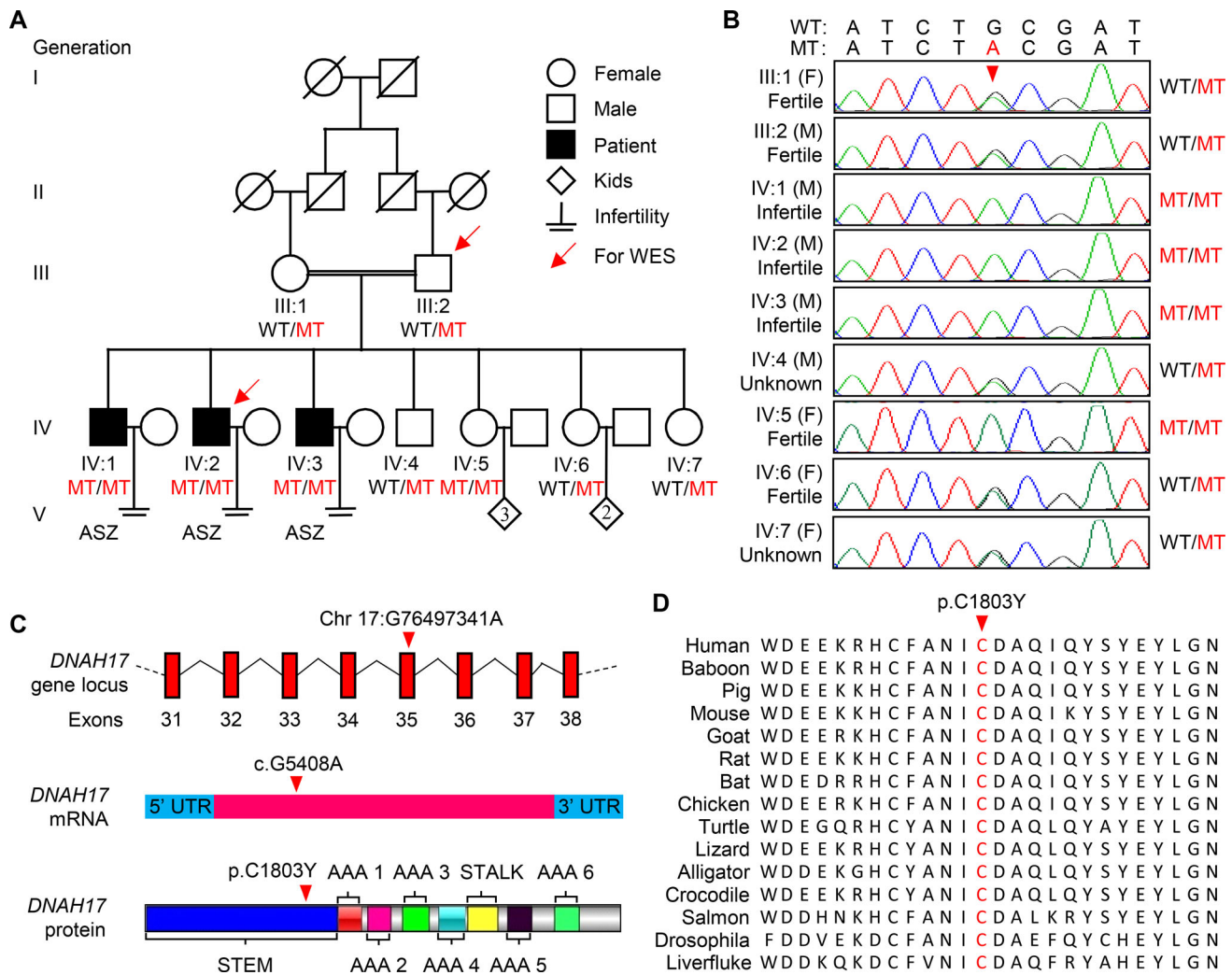


Figure 1. **A** *DNAH17* missense variant in a consanguineous Pakistani family with asthenozoospermia. **(A)** Pedigree of the consanguineous family with three asthenozoospermia patients (IV:1, IV:2, and IV:3). Arrows point to the two individuals for whom WES was performed. Slashes denote deceased family members, and the double horizontal lines represent consanguineous marriage. ASZ, asthenozoospermia. **(B)** Chromatograms of the *DNAH17* missense mutation (g.G78136A) in genomic DNA from all the available family members. F, female; M, male. **(C)** The *DNAH17* mutation occurs in exon 35 and causes a G-to-A substitution at cDNA (NCBI reference sequence no. NM_173628) nucleotide position 5408, replacing cysteine (C) with tyrosine (Y) at amino acid 1803 in the *DNAH17* protein (UniProt accession no. Q9UFH2). **(D)** Sequence alignment shows conservation of the affected amino acid (cysteine) across different organisms. Arrowheads, the mutation site; WT, the wild-type allele; MT, the mutant allele; UTR, untranslated region.

The specificity of the antibody was further validated in *Dnah17*^{-/-} mice that were generated using the CRISPR/Cas9 technique (Fig. S3 C). Immunoblotting using the antibody against *DNAH17* detected a specific band at the predicted size of *DNAH17* protein in sperm lysates from *Dnah17*^{+/-} mice, but not in sperm lysates of *Dnah17*^{-/-} mice (Fig. S3 D). Similarly, IF staining of spermatozoa from *Dnah17*^{+/-} mice showed clear and specific signals of *DNAH17* colocalizing with α -tubulin, one of the major constituents of microtubules (Amos and Klug, 1974), along sperm tails except the distal tip, but the signals of anti-*DNAH17* antibody were completely absent in sperm flagella from *Dnah17*^{-/-} mice (Fig. S3 E). Noticeably, knockout of *Dnah17* drastically reduced sperm count and resulted in morphologically abnormal spermatozoa with a typical human MMAF phenotype (Fig. S3, F-I). The 9+2 axonemal configuration was completely disrupted in flagella of *Dnah17*^{-/-} mice (Fig. S3 J).

These in vitro and in vivo studies collectively indicated that, although the anti-*DNAH17* antibody could cross-react with the epitope-corresponding peptides of *DNAH9* and *DNAH11* over-expressed in cultured cells, it is not likely to recognize endogenous *DNAH9* and *DNAH11* proteins in mice and humans.

The expression and localization of *DNAH17*

In mice, *Dnah17* mRNA was abundantly expressed in testes but not detected in lungs, tracheae, or oviducts (Fig. 2 C). Using the antibody against *DNAH17*, we found that *DNAH17* protein was indeed not detected in cilia from tracheae and was detected only in testes and epididymides of WT mice (Fig. 2, A, D, and E), but not in epididymides of *Rpl10l*^{-/-} mice devoid of spermatozoa (Fig. 2 E; Jiang et al., 2017), indicating that *DNAH17* expression is restricted to testes and spermatozoa. IF staining further showed that *DNAH17* is localized predominantly in cytoplasm and

Table 1. **Clinical characteristics of patients**

	Reference values ^a	IV:1	IV:2	IV:3
Genotype		MT/MT	MT/MT	MT/MT
Age (years) ^b		43	41	29
Years of marriage ^c		20	17	11
Height/weight (cm/kg)		182.9/70.0	167.6/70.0	167.6/50.0
Semen parameters				
Semen volume (ml)	>1.5	3.3 ± 0.9	2.0 ± 1.0	3.5 ± 0.7
Semen pH	Alkaline	Alkaline	Alkaline	Alkaline
Sperm concentration (10 ⁶ /ml)	>15	18.0 ± 1.4	30.0 ± 0	17.3 ± 1.6
Morphologically normal sperm (%)	>4	76.8 ± 2.8	83.8 ± 0.3	78.4 ± 0.5
Motile sperm (%)	>40	11.5 ± 4.6	25.0 ± 10.6	15.1 ± 5.0
Progressively motile sperm (%)	>32	5.5 ± 1.8	17.5 ± 8.8	9.4 ± 3.1

Two independent experiments were performed. Data are presented as mean ± SEM. MT, the mutant allele.

^aReference values were published in WHO (2010).

^bThe current ages.

^cThe current years of marriage.

flagella of step 11–16 spermatids of adult mice (Fig. 2 F). Consistently, in humans, DNAH17 was detected only in testes, but not in various somatic cell lines (Fig. 2 G and Fig. S3 K). Immunohistochemical staining on human testicular sections with normal spermatogenesis revealed that DNAH17 could be detected in cytoplasm and flagella of elongated spermatids (Fig. 2 H). IF staining on human semen smears showed localization of DNAH17 in sperm flagella (Fig. 2 I). Together, the expression and localization patterns of DNAH17 propose its potential role in spermatozoa.

Localization of the mutant DNAH17 in patients

To explore whether the identified variant affected expression and localization of DNAH17 in patients, we performed IF staining on semen smears using the anti-DNAH17 antibody. The signals of DNAH17 and α -tubulin were detected in sperm flagella of all three patients and were not distinguishable from those in the fertile controls (Fig. 3).

Morphological and ultrastructural analyses of sperm flagella from patients

Since mutations in *DNAH1*, another member of the DNAH family, have been reported to be associated with the MMAF phenotype (Coutton et al., 2018; Ben Khelifa et al., 2014; Sha et al., 2017; Tang et al., 2017; Wang et al., 2017), to understand whether this *DNAH17* variant could also induce an MMAF-like phenotype, we conducted further examinations of sperm morphology for all three patients. Semen samples from a fertile man with normal spermogram were used as the control. There was no significant difference in the percentage of abnormalities in sperm head, tail, or head and tail between patients and control (Fig. S4, A and B). Moreover, spermatozoa were classified into six subtypes according to flagellar morphology, including normal, absent, bent, short, coiled, and irregular-caliber flagella (Ben Khelifa et al., 2014). The flagella of >80% of spermatozoa in the patients

were morphologically normal, and the frequency of each type of flagella in the patients did not significantly differ from that in the control (Fig. S4 C). Hence, all three patients did not present with the MMAF phenotype.

We next examined whether the axonemal structure of sperm tails, the horsepower apparatus that drives sperm “swimming,” was impaired by the *DNAH17* variant (Inaba, 2011; Roberts et al., 2013). Transmission EM (TEM) analyses of sperm flagella were performed. In all three patients, cross sections of midpiece displayed a typical 9+2 axonemal configuration (Fig. 4 A). However, all three patients exhibited a frequent absence of MTD(s) 4–7, accounting for $\geq 39.7\%$ and $\geq 60.3\%$ of all cross sections at principal piece and end piece, respectively, which were significantly higher than those in controls (2.2% at principal piece and 1.0% at end piece; Fig. 4, A and B; and Fig. S4 D). Interestingly, the associated outer dense fibers (ODFs) were also absent in the cross sections with MTD(s) 4–7 missing in our patients. Further examination of the ultrastructural anomalies in the three patients revealed that the simultaneous loss of MTDs 4–7 was most frequently observed ($\geq 32.6\%$ and $\geq 46.9\%$ of all cross sections at principal piece and end piece, respectively; Fig. 4, A, C, and D). Besides missing MTD(s) 4–7, other abnormalities, such as disorganization of MTDs, excess microtubules, missing almost all the microtubules, etc., were also observed in patients at low frequencies, which were not significantly different from those in controls (Fig. 4 E). Intriguingly, the ODA was clearly observed attached to each of the nine MTDs at midpiece and to each of the remaining MTDs at principal piece and end piece in all three patients (Fig. 4 A). Taken together, these findings indicate that the impaired sperm motility in patients was likely due to the loss of MTD(s) 4–7 at principal piece and end piece of sperm flagella.

Diminished sperm motility in *Dnah17^{M/M}* mice

Given the 91% identity in amino acid sequence (Fig. S2) and the same expression and localization patterns of DNAH17 between

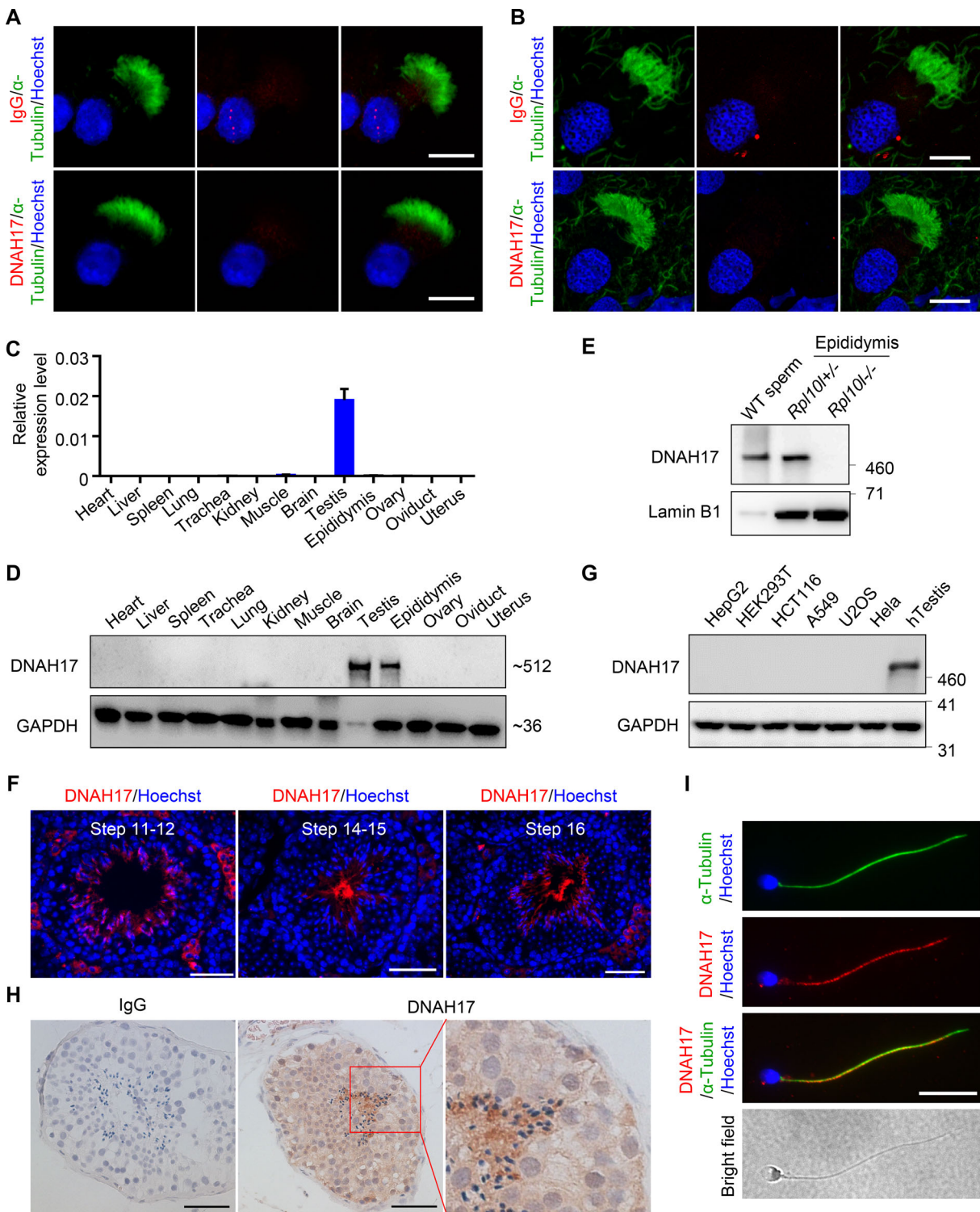


Figure 2. Expression and localization of DNAH17 in humans and mice. (A and B) Representative images of mouse (A) and human (B) respiratory cilia stained for α -tubulin (a marker for the ciliary axoneme) and rabbit IgG (negative control, upper panel) or DNAH17 (lower panel). Scale bars represent 10 μ m. **(C)** Quantitative real-time PCR analysis of *Dnah17* mRNA expression in adult mouse tissues. *Actb* was used as an internal control. **(D)** Immunoblotting analysis of DNAH17 protein in different tissues from adult mice. GAPDH was used as the loading control. **(E)** Immunoblotting with sperm lysates from WT mice and epididymal lysates from *Rpl10l*^{+/-} and *Rpl10l*^{-/-} mice using the anti-DNAH17 antibody. Lamin B1 was used as the loading control. **(F)** Representative images of testicular tubules stained with anti-DNAH17 antibody and Hoechst showing that DNAH17 is localized in the cytoplasm and flagella of step 11–16 spermatids. Scale bars represent 50 μ m. **(G)** Immunoblotting with lysates of human cell lines HepG2 (from liver), HEK293T (from embryonic kidney), HCT116 (from colon), A549 (from alveolar basal epithelia), U2OS (from bone), HeLa (from cervix), and adult human testes (hTestis) using the anti-DNAH17 antibody. GAPDH was used as the loading control. **(H)** Immunohistochemistry using the anti-DNAH17 antibody on adult human testicular sections with normal spermatogenesis. Rabbit IgG (left panel) was used as a negative control. Scale bars represent 50 μ m. **(I)** Representative images of spermatozoa from fertile men (controls) stained with anti-DNAH17 antibody, anti- α -tubulin antibody, and Hoechst. Scale bar represents 10 μ m. For A–I, three independent experiments were performed.

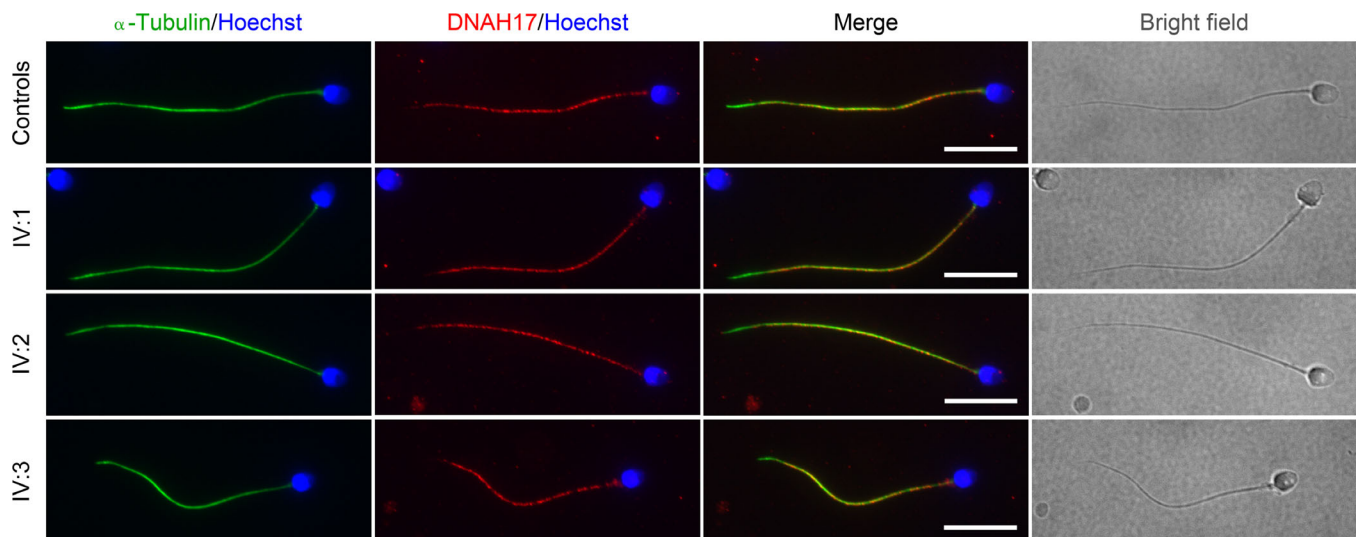


Figure 3. Localization of the mutant DNAH17 is not altered in patients. Representative images of spermatozoa from fertile controls and three patients stained with the anti-DNAH17 antibody, anti- α -tubulin antibody, and Hoechst. Two independent experiments were performed, and at least 150 sperm were examined for each time per individual. Scale bars represent 10 μ m.

human and mouse (Fig. 2), to functionally verify whether the DNAH17 variant was indeed the pathogenic variant for the defects in patients' sperm tails, we generated a mouse model (*Dnah17^{M/M}*) that carried a homozygous *Dnah17* c.G5360A mutation (Fig. S5, A–C) equivalent to the DNAH17 variant (c.G5408A) in patients, using CRISPR/Cas9-mediated genome editing.

Dnah17^{M/M} male mice were subfertile, with an ~64.8% reduction in litter size per pair compared with controls (Table 2). Further examination showed that body weight, testis weight and their ratio, testicular histology, sperm count, and sperm morphology (particularly the frequencies of morphological normal flagella and each type of abnormal flagella) in *Dnah17^{M/M}* or *Dnah17^{+/M}* mice were all comparable to those in *Dnah17^{+/+}* mice (Table 2 and Fig. S5, D and E). The percentages of motile and progressively motile sperm showed no significant difference between *Dnah17^{+/M}* mice and controls, but they were dramatically decreased in *Dnah17^{M/M}* mice (Table 2). Hence, consistent with the findings in the patients (Table 1), *Dnah17^{M/M}* mice displayed markedly diminished sperm motility, proving that the DNAH17 variant is indeed pathogenic for asthenozoospermia.

Ultrastructure of sperm flagella from *Dnah17^{M/M}* mice

To understand whether the ultrastructure of sperm flagella in mice was also altered by the DNAH17 variant, TEM analyses of flagella of spermatozoa isolated from cauda epididymides were conducted. Cross sections of midpiece from both *Dnah17^{+/+}* and *Dnah17^{M/M}* mice exhibited classical 9+2 axonemal configuration. Nonetheless, 42.9% and 87.2% of cross sections of principal piece and end piece, respectively, showed MTD(s) 4–7 missing with a concomitant loss of the associated ODF(s) in *Dnah17^{M/M}* mice, in sharp contrast to 0.6% and 1.7%, respectively, in controls (Fig. 5, A and B). Consistent with the observations in patients, the most frequent anomaly in *Dnah17^{M/M}* mice was the simultaneous absence of MTDs 4–7, accounting for 21.1% and 54.9% of all cross

sections at principal piece and end piece, respectively (Fig. 5, A, C, and D). Moreover, the absence of MTD 4 or 7 was detected at lower frequencies (Fig. 5, C–E). Though some abnormalities other than the lack of MTD(s) 4–7 were also observed in flagellar cross sections of *Dnah17^{M/M}* and control mice, their percentages were low and showed no significant difference (Fig. 5 F). It is also worth noting that the ODA attached to each of the remaining MTDs was visible on all the cross sections examined for *Dnah17^{M/M}* mice (Fig. 5 A). Together, these TEM findings in *Dnah17^{M/M}* mice recapitulated the defects of patients' sperm tails, demonstrating that the DNAH17 variant was indeed responsible for the absence of MTD(s) 4–7 in our asthenozoospermic patients.

MTDs 4–7 were destabilized in cauda epididymis

The frequent absence of MTD(s) 4–7 observed in spermatozoa from both patients and *Dnah17^{M/M}* mice could be due to either defective flagellum biogenesis or MTD destabilization. TEM analyses of the sperm flagella in seminiferous tubules retrieved from testes were performed and revealed that abnormal axoneme structure was not observed in all cross sections examined for *Dnah17^{M/M}* mice (Fig. 6, A and B), indicating that the cause of MTD(s) 4–7 absence was not a defect in axonemal assembly.

To investigate whether the lack of MTD(s) 4–7 occurred during transition of spermatozoa, we performed TEM analyses of spermatozoa within caput, corpus, and cauda epididymides and found that axonemal structure abnormality was hardly detected in all cross sections examined for *Dnah17^{M/M}* caput and corpus epididymides (Fig. 6, C–F). However, flagella in *Dnah17^{M/M}* cauda epididymides displayed significantly higher frequencies of abnormal axoneme structure at principal piece and end piece than in controls (Fig. 6, G and H). Interestingly, in *Dnah17^{M/M}* cauda epididymides, 33.8% and 85.3% of cross sections at principal piece and end piece, respectively, presented with MTD(s) 4–7 missing, while only 1.7% and 0.9%, respectively, were detected with such abnormalities in controls (Fig. 6 I). The

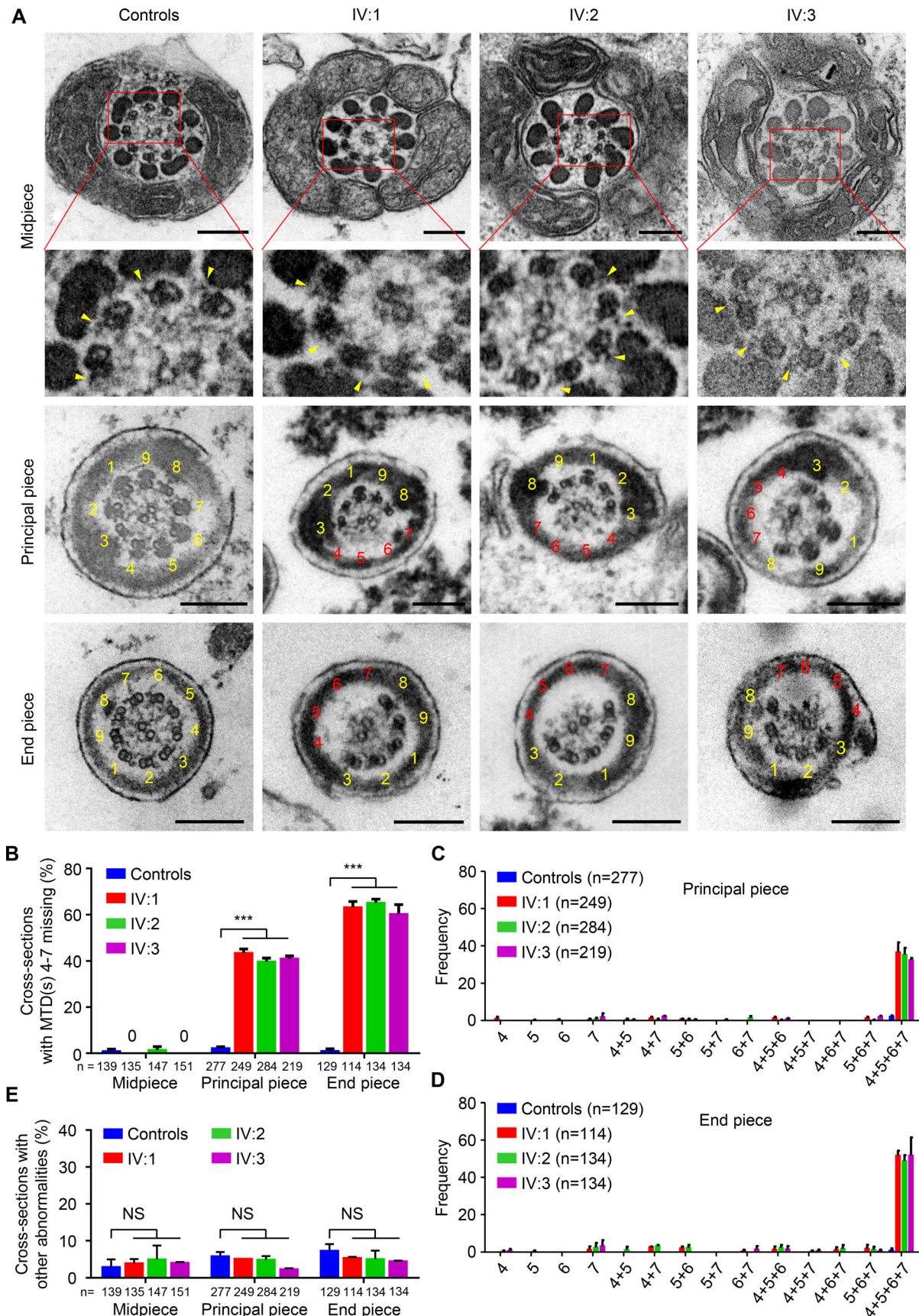


Figure 4. **Sperm flagella from patients show frequent absence of MTDs 4–7 at principal piece and end piece.** (A) Representative TEM micrographs showing cross sections of midpiece, principal piece, and end piece of sperm flagella from fertile men (controls) and three patients. Numbers in yellow indicate

the MTDs with typical arrangement, numbers in red indicate the missing MTDs, and arrowheads highlight the ODAs. Scale bars represent 200 nm. **(B)** Quantification of flagella with loss of any combination of MTDs 4–7 at midpiece, principal piece, and end piece from controls and three patients. **(C and D)** The percentages of cross sections with MTD(s) 4, 5, 6, 7, 4+5, 4+7, 5+6, 5+7, 6+7, 4+5+6, 4+5+7, 4+6+7, 5+6+7, or 4+5+6+7 missing at principal piece (C) and end piece (D). **(E)** Quantification of cross sections with abnormalities other than the MTD(s) 4–7 missing at midpiece, principal piece, and end piece of sperm flagella from controls and three patients. Two independent experiments were performed. n, the number of axonemal cross sections analyzed. Data are presented as mean \pm SEM. ***P < 0.001; one-way ANOVA test.

levels of α -tubulin, β -tubulin, and DNAH17 in lysates of sperm from cauda epididymides were further evaluated and found to be comparable between *Dnah17^{M/M}* and control mice (Fig. 6 J), indicating that these proteins were not degraded and the lack of MTD(s) 4–7 could be due to destabilization. Hence, these findings revealed that the structural defects of sperm flagella observed in patients and *Dnah17^{M/M}* mice could result from the destabilization of MTDs 4–7 occurring specifically in cauda epididymis.

Destabilization of MTDs 4–7 is related to the storage of sperm in epididymides

Since cauda epididymis is the place where spermatozoa are stored before ejaculation, we thus examined whether the storage

time could predispose MTDs 4–7 to destabilization. We conducted epididymal duct ligation at the end of corpus adjacent to cauda for 2 d and 4 d, respectively (Fig. 7 A), simulating the different lengths of time that spermatozoa were stored in epididymides. 2 or 4 d after ligation, a large number of spermatozoa were accumulated in the corpus region in both WT and *Dnah17^{M/M}* mice (Fig. S5 F). TEM analyses of flagella of sperm in the corpus were subsequently performed. Compared with WT mice, significantly increased frequencies of MTD(s) 4–7 missing at the principal piece (16.5%) and end piece (59.1%) were observed in *Dnah17^{M/M}* mice 2 d after ligation (Fig. 7, B and C). 4 d after ligation, the frequencies were further increased to 24.2% at principal piece and 82.7% at end piece in *Dnah17^{M/M}* mice, while

Table 2. Characteristics of *Dnah17^{+/+}*, *Dnah17^{+/M}*, and *Dnah17^{M/M}* male mice

Parameters	<i>Dnah17^{+/+}</i>	<i>Dnah17^{+/M}</i>	<i>Dnah17^{M/M}</i>
Body weight (g)	27.0 \pm 0.5	26.1 \pm 1.0 ^a	26.3 \pm 0.8 ^a
Testis weight (mg)	164.5 \pm 3.3	167.4 \pm 0.4 ^a	176.2 \pm 8.9 ^a
Testis/body weight ratio (10 ⁻³)	6.1 \pm 0.1	6.4 \pm 0.2 ^a	6.7 \pm 0.2 ^a
Fertility			
No. of fertile/total mice	3/3	3/3	5/5
Pups per fertile pair	24.7 \pm 0.3	24.2 \pm 0.2 ^a	8.7 \pm 0.5***
Semen parameters			
Sperm count (10 ⁷)	1.4 \pm 0.1	1.4 \pm 0.1 ^a	1.3 \pm 0.1 ^a
Motile sperm (%)	76.7 \pm 1.2	72.7 \pm 0.9 ^a	19.8 \pm 3.4***
Progressively motile sperm (%)	32.7 \pm 0.3	35.0 \pm 1.2 ^a	9.2 \pm 2.0***
Sperm morphology			
Morphologically normal (%)	88.9 \pm 0.6	89.3 \pm 0.7 ^a	90.4 \pm 0.6 ^a
Abnormal head (%)	1.9 \pm 0.6	3.4 \pm 0.4 ^a	2.3 \pm 1.0 ^a
Abnormal tail (%)	5.9 \pm 0.6	4.0 \pm 0.7 ^a	4.2 \pm 0.7 ^a
Abnormal head and tail (%)	3.3 \pm 0.7	3.3 \pm 0.5 ^a	3.1 \pm 0.2 ^a
Sperm flagella^b			
Morphologically normal (%)	90.9 \pm 0.5	92.7 \pm 0.8 ^a	92.5 \pm 0.6 ^a
Absent (%)	2.4 \pm 0.4	1.9 \pm 0.3 ^a	1.6 \pm 0.3 ^a
Short (%)	1.1 \pm 0.4	1.0 \pm 0 ^a	1.1 \pm 0.1 ^a
Coiled (%)	3.0 \pm 0.9	2.4 \pm 0.7 ^a	2.8 \pm 0.6 ^a
Bent (%)	1.0 \pm 0.3	1.0 \pm 0.3 ^a	0.8 \pm 0.1 ^a
Irregular caliber (%)	1.6 \pm 0.1	1.0 \pm 0.3 ^a	1.2 \pm 0.3 ^a

For fertility test, three *Dnah17^{+/+}*, three *Dnah17^{+/M}*, and five *Dnah17^{M/M}* male mice (10 wk old) were each caged with two WT females (C57BL/6J; 10 wk old) for 90 d. For semen analysis, three 10-wk-old mice were examined for each genotype. Data are presented as mean \pm SEM. ***P < 0.001; compared with the *Dnah17^{+/+}* mice, one-way ANOVA with Dunnett's multiple comparison test.

^aNS, not significant.

^bEach spermatozoon was classified as only one type of flagellar morphology according to its major abnormality.

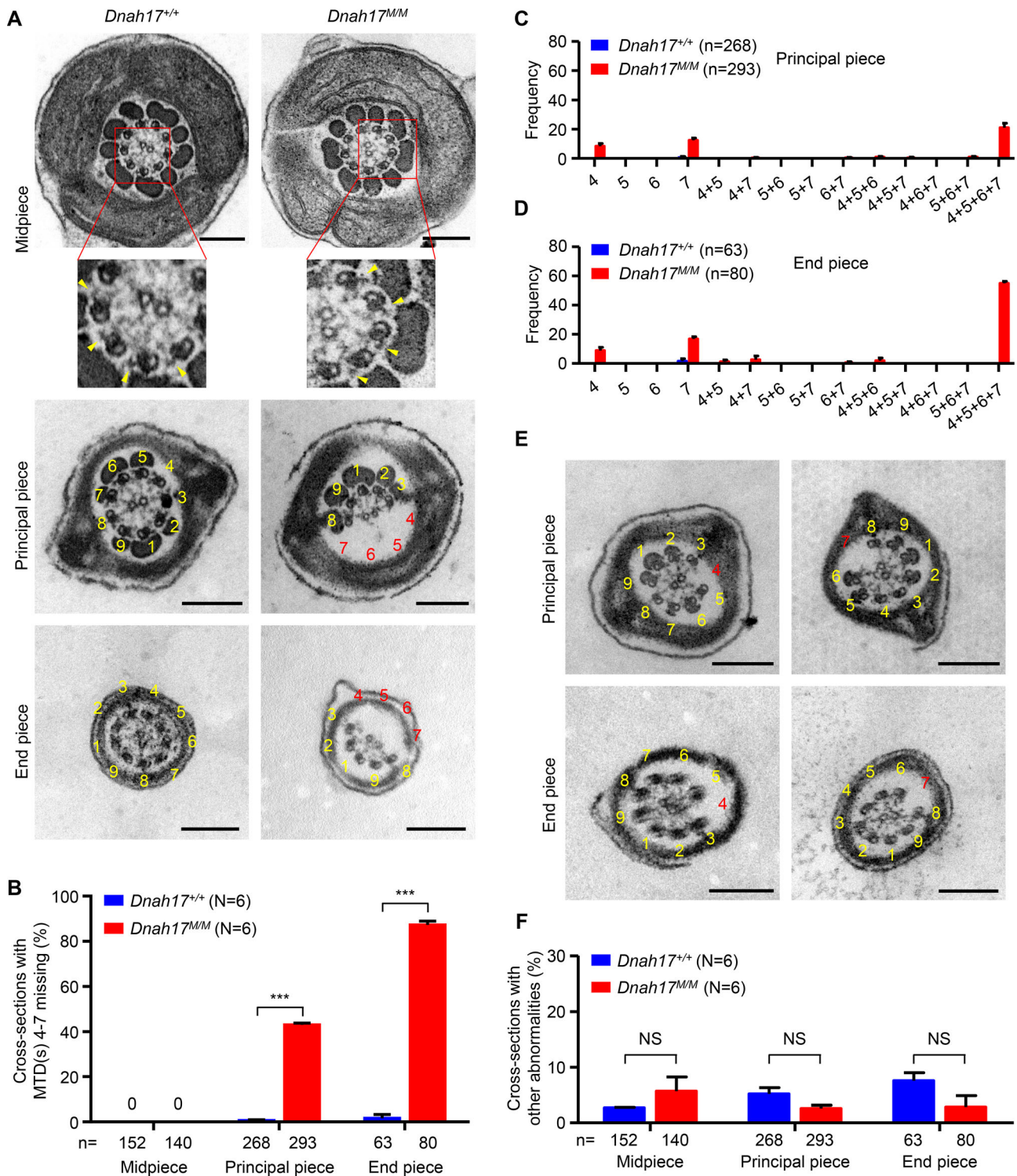


Figure 5. **Sperm flagella from *Dnah17^{MM}* mice show frequent absence of MTDs 4–7 at principal piece and end piece.** (A) Representative TEM micrographs showing cross sections of midpiece, principal piece, and end piece of sperm flagella from *Dnah17^{+/+}* and *Dnah17^{MM}* mice. (B) Percentages of the flagellar cross sections with loss of any combination of MTDs 4–7 at midpiece, principal piece, and end piece. (C and D) Frequencies of cross sections with MTD(s) 4, 5, 6, 7, 4+5, 4+7, 5+6, 5+7, 6+7, 4+5+6, 4+5+7, 4+6+7, 5+6+7, or 4+5+6+7 missing at principal piece (C) and end piece (D) from *Dnah17^{+/+}* and *Dnah17^{MM}* mice. (E) Representative cross sections with MTD 4 or 7 missing at principal piece and end piece of sperm flagella from *Dnah17^{MM}* mice. (F) Percentages of flagellar cross sections with abnormalities other than MTD(s) 4–7 missing. For A and E, numbers in yellow indicate the MTDs with typical arrangement, numbers in red indicate the missing MTDs, and arrowheads highlight the ODAs; scale bars represent 200 nm. N, the number of mice examined. n, the number of axonemal cross sections analyzed. Data are presented as mean ± SEM. ***P < 0.001; Student's t test.

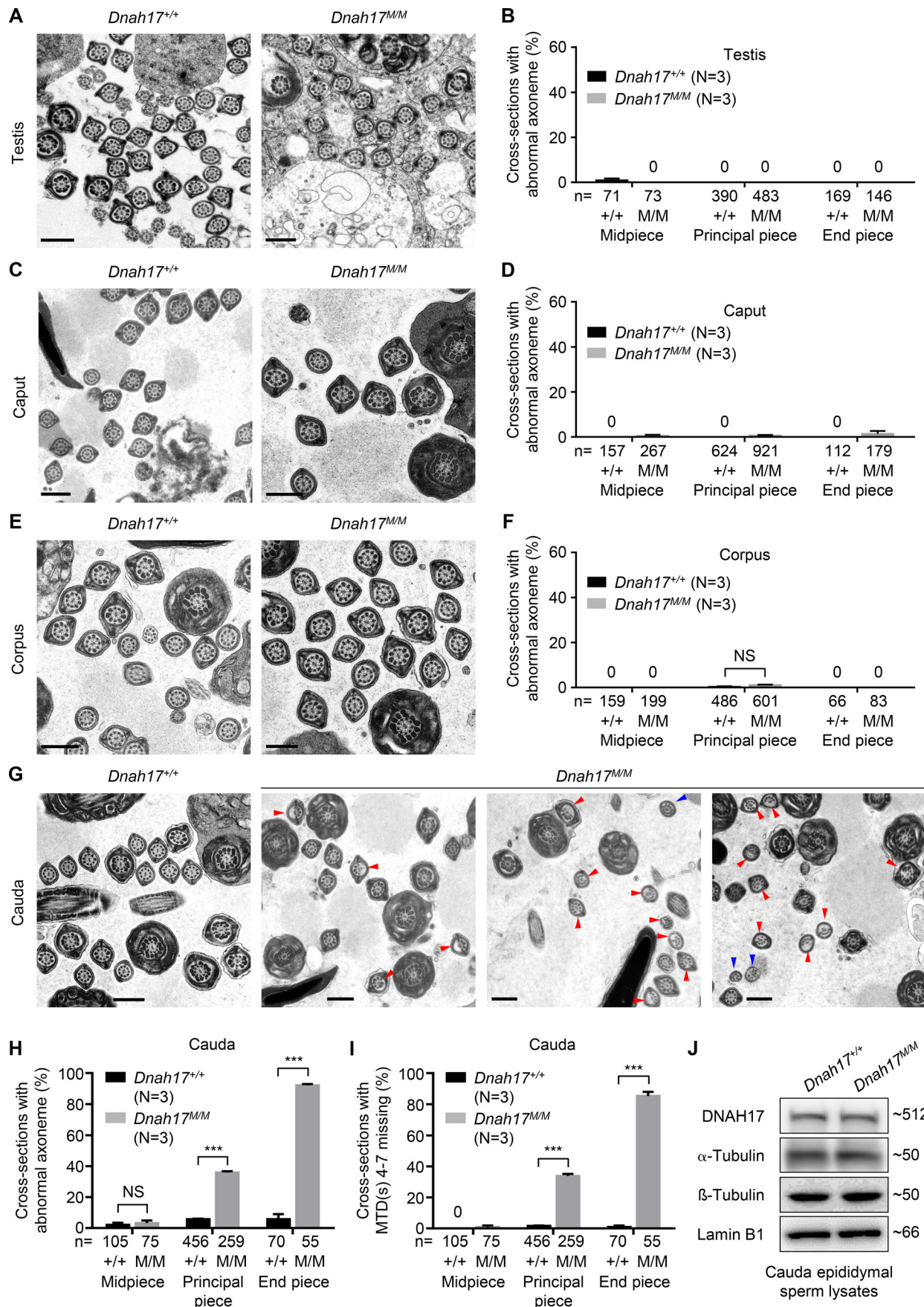


Figure 6. MTDs 4–7 are destabilized in cauda epididymides of *Dnah17^{M/M}* mice. (A) Representative TEM micrographs of flagellar cross sections in testes from *Dnah17^{+/+}* and *Dnah17^{M/M}* mice. **(B)** The percentages of cross sections with abnormal axoneme structure (including anomalies related to MTDs 4–7 and other anomalies) in testes from *Dnah17^{+/+}* and *Dnah17^{M/M}* mice. **(C–H)** Representative TEM micrographs of flagellar cross sections and the percentages of cross sections with abnormal axoneme structure in caput (C and D), corpus (E and F), and cauda (G and H) epididymides from *Dnah17^{+/+}* and *Dnah17^{M/M}* mice. Red arrowheads, cross sections with loss of any combination of MTDs 4–7; blue arrowheads, cross sections with axonemal abnormalities other than the loss of MTD(s) 4–7. Scale bars represent 500 nm. **(I)** The percentages of cross sections with loss of any combination of MTDs 4–7 in cauda epididymides of *Dnah17^{+/+}* and *Dnah17^{M/M}* mice. **(J)** Immunoblotting with lysates of spermatozoa from cauda epididymides using anti-DNAH17, anti- α -tubulin, and anti- β -tubulin antibodies. Lamin B1 was used as the loading control. Three independent experiments were performed. N, the number of mice analyzed. n, the number of axonemal cross sections analyzed. Data are presented as mean \pm SEM. *** $P < 0.001$; Student's *t* test.

the frequencies in control mice remained very low (Fig. 7, B and C). These observations indicate that MTDs 4–7 destabilization is negatively associated with the length of ligation time. Thus, combined with the findings on flagellar structure of sperm in cauda epididymides (Fig. 6, G–I), we proposed that the destabilization of MTDs 4–7 in *Dnah17^{M/M}* mice is most probably due to storage of sperm in epididymides, regardless of storage in corpus or cauda.

Discussion

Our study identifies a homozygous missense variant (c.G5408A) in *DNAH17*, a functionally uncharacterized gene, from a consanguineous Pakistani family with three offspring suffering from asthenozoospermia (no MMAF-like phenotype) and provides genetic evidence that *DNAH17* c.G5408A is pathogenic for asthenozoospermia using *Dnah17^{M/M}* mice modeling the patients' mutation. Extensive examinations of the spermatozoa from the three patients and *Dnah17^{M/M}* mice collectively elucidate that the *DNAH17* variant causes frequent absence of MTD(s) 4–7 at principal piece and end piece during the sperm storage in epididymides. Thus, we demonstrate for the first time that *DNAH17* is essential for sperm motility, and is the only known DNAH protein implicated in stabilizing flagellar structure, specifically MTDs 4–7.

Eukaryotic cilia and sperm flagella share a highly conserved 9+2 axonemal structure, constituted of microtubules, motor dynein arms, and their associated structures. Thus, it is not surprising that a multitude of mutations in genes encoding axonemal machinery has been identified in humans that are commonly linked to PCD and asthenozoospermia (Ji et al., 2017). All the family members in our study declared not having any ciliary-related symptoms and thus refused to participate in any further related examination. One sister (IV:5), who is homozygous for the *DNAH17* variant, had three children and no miscarriages, suggesting that *DNAH17* may be dispensable for ciliary functions. Furthermore, we found that both human and mouse *DNAH17* is highly expressed in testes and spermatozoa, but was not detected in respiratory cilia, indicating that *DNAH17* is required only for flagella but not cilia. Hence, we conclude that the *DNAH17* variant causes isolated asthenozoospermia without any other PCD-related symptoms.

DNAH17, along with *DNAH9* and *DNAH11*, is a homologue of *C. reinhardtii* ODA β -HCs in mammals (Pazour et al., 2006). Different from the testis/spermatozoa-restricted expression pattern for *DNAH17*, *DNAH9* and *DNAH11* are localized to the

distal and proximal regions of respiratory ciliary axonemes, respectively (Dougherty et al., 2016; Fliegauf et al., 2005). Besides, *DNAH9* was also found localized through the sperm flagella except the distal tip (Fliegauf et al., 2005), which is similar to *DNAH17* localization in sperm flagella. Biallelic mutations in *DNAH9* cause PCD with a frequent loss of ODAs at the distal, but not the proximal, regions of cilia (Fassad et al., 2018; Loges et al., 2018), and the patient carrying two homozygous missense mutations in *DNAH9* presented with oligoasthenoteratozoospermia (Fassad et al., 2018), yet the underlying ultrastructural anomalies and pathogenic mechanism remain unknown. Biallelic mutations in *DNAH11* in patients are known to cause PCD without obvious defects in the ciliary ultrastructure; however, the sperm motility, flagellar ultrastructure, and fertility status of these patients were not mentioned (Bartoloni et al., 2002; Knowles et al., 2012; Lucas et al., 2012; Pifferi et al., 2010; Schwabe et al., 2008), with the exception of one man, who had one child without the use of medical assistance (Schwabe et al., 2008). The mouse model carrying a mutation (E2271K) in *Dnah11* displayed reduced fertility and sperm motility, though the ultrastructure of sperm tails appeared normal (Lucas et al., 2012). Hence, it remains uncertain whether *DNAH11* is required for male fertility. Future studies are needed to further explore the roles of *DNAH11* and *DNAH9* in sperm tails.

Disruptions in flagellar axoneme proteins have been reported to be associated with MMAF in humans (Martinez et al., 2018). Thus, it is not surprising that knockout of *Dnah17* induced an MMAF phenotype, which likely resulted from defective flagellar biogenesis. Noticeably, *Dnah17^{M/M}* mice displayed a normal flagellar biogenesis but destabilized MTDs 4–7 during epididymal sperm storage, which is a unique phenotype that has not been reported so far in human or animal mutants for any other DNAHs (Ben Khelifa et al., 2014; Lucas et al., 2012; Neesen et al., 2001; Sha et al., 2017; Wang et al., 2017; Zuccarello et al., 2008). It is implied that the *Dnah17* missense mutation is less deleterious than *Dnah17* knockout, thus allowing the identification of the indispensable role of *DNAH17* in stabilizing MTDs 4–7 during sperm storage in epididymis. We have also tried to detect whether there was a frequent loss of MTD(s) 4–7 in *Dnah17^{-/-}* mice, but the flagellar axoneme structures were so disorganized that we were unable to determine the order of MTDs in *Dnah17^{-/-}* mice. Taken together, the phenotypic difference between *Dnah17^{-/-}* mice and our patients or *Dnah17^{M/M}* mice indicates that *DNAH17* is required for both flagellar biogenesis during spermiogenesis and stabilizing MTDs 4–7 during sperm storage in epididymis. It would be interesting to know whether

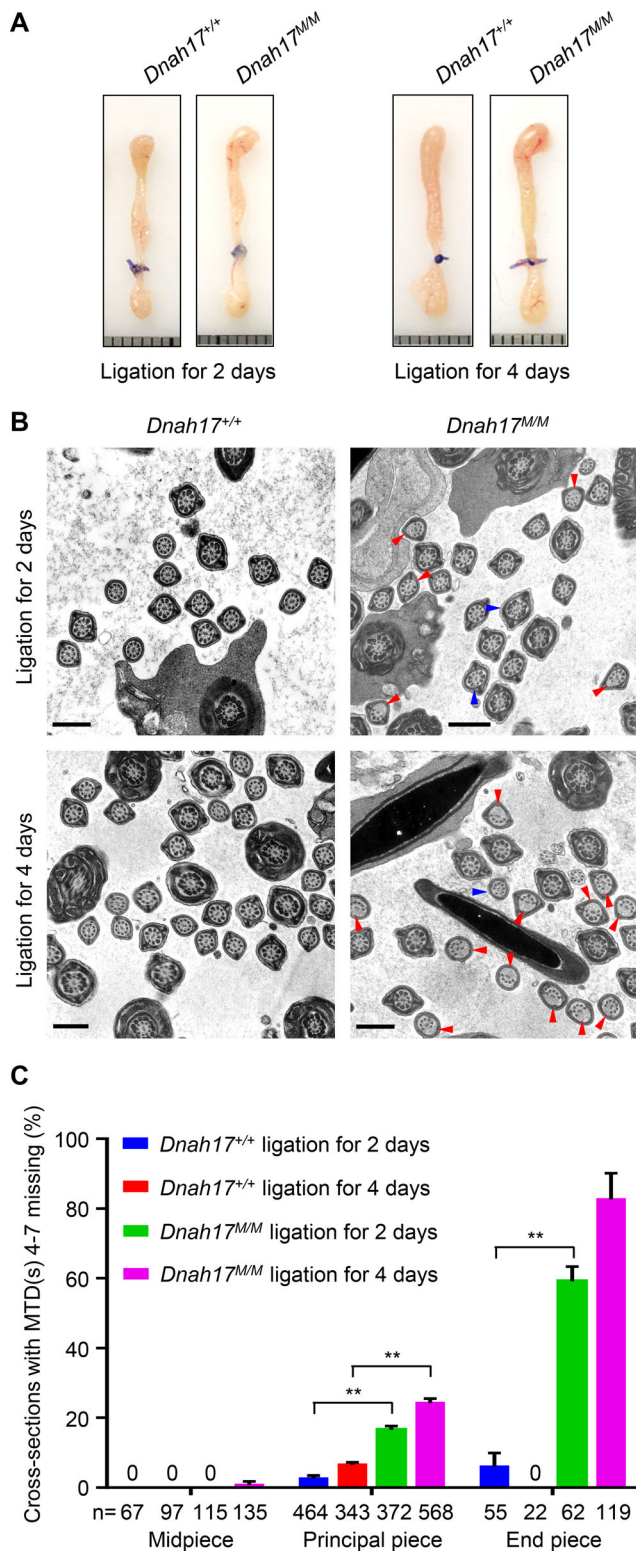


Figure 7. TEM analyses of sperm flagella in corpus epididymides after epididymal duct ligation. (A) Representative images of epididymides from *Dnah17^{+/+}* and *Dnah17^{MM}* mice after ligation for 2 d and 4 d. The epididymal ducts were ligated at the end of corpus adjacent to cauda. Each grid represents 1 mm. **(B)** Representative TEM micrographs of flagellar cross sections in corpus epididymides after ligation for 2 d and 4 d. Red arrowheads indicate cross sections with loss of any combination of MTDs 4–7, and blue arrowheads indicate cross sections with axonemal abnormalities other than the

other axoneme proteins are also implicated in stabilizing axonemal structures and their mutation frequency in asthenozoospermic patients with ultrastructure defects but normal morphology of flagella, which have not been paid enough attention in the past.

After leaving the testis, sperm entered the caput epididymis, progressing to corpus, and finally reached the cauda, where they were stored until ejaculation. Here, we found that, when sperm were kept in corpus for 2 or 4 d, MTDs 4–7 were also destabilized in *Dnah17^{MM}* mice, showing a time-dependent manner. Noticeably, at the end piece, the frequency of MTD(s) 4–7 missing in the corpus of *Dnah17^{MM}* mice with epididymal duct ligated for 4 d was similar to that in the cauda of unligated *Dnah17^{MM}* mice; however, at the principal piece, the frequency in *Dnah17^{MM}* corpus after ligation for 4 d remained significantly less than that in the cauda of unligated *Dnah17^{MM}* mice. These findings not only indicate that MTDs 4–7 at the end piece could be more susceptible to destabilization than those at principal piece, but also imply that the destabilization likely occurs from the distal region of the flagellum. There are two possible explanations for why MTD(s) 4–7 at principal piece were more prone to destabilization in the cauda of unligated mice than in the corpus after ligation for 4 d. First, the destabilization of doublets at principal piece may need a longer time than those at end piece. In unligated mice, sperm could be stored in the cauda epididymis for >4 d, as the densities of sperm in the corpus lumen 4 d after ligation (Fig. S5 F) were obviously lower than those in the cauda from unligated mice (Fig. S5 E). Second, the relatively lower pH and ionic calcium concentration and higher osmotic pressure in the lumen of cauda than in corpus (Dacheux and Dacheux, 2013; Shum et al., 2009; Turner, 2008) may also contribute to the instability of MTD(s) 4–7. Consistently, previous studies have shown that the disruption of *Pla2g3* (Sato et al., 2010), *Ttll9* (Konno et al., 2016), or *Vdac3* (Sampson et al., 2001) also induced instability of MTDs 4–7 or MTD 7 in mouse cauda epididymides. Together, these pieces of evidence led us to believe that MTDs 4–7 are different from the other MTDs, and must be armed with delicate machinery to cope with the prolonged storage and possible environmental challenges in epididymis. Therefore, future efforts should be attempted to interrogate the compositional, structural, and functional differences between MTDs 4–7 and the other MTDs. Moreover, the ultrastructural localization of DNAH17 in flagellar axoneme and interacting proteins of DNAH17 need to be elucidated in the future with antibodies suitable for use in immunoelectron microscopy and co-immunoprecipitation, to decipher the specific and interesting role of DNAH17 in stabilizing MTDs 4–7.

In conclusion, we demonstrated that a homozygous *DNAH17* missense variant specifically induces MTDs 4–7 destabilization in cauda epididymis, resulting in asthenozoospermia. It would

loss of MTD(s) 4–7. Scale bars represent 500 nm. **(C)** The percentages of cross sections with loss of any combination of MTDs 4–7 in corpus epididymides of *Dnah17^{+/+}* and *Dnah17^{MM}* mice. Two independent experiments were performed. n, the number of axonemal cross sections analyzed. Data are presented as mean ± SEM. **P < 0.01; one-way ANOVA test.

3518–3817, mouse DNAH17 amino acids 3502–3801, human DNAH11 (amino acids 3572–3871), mouse DNAH11 (amino acids 3544–3843), human DNAH9 (amino acids 3542–3841), or mouse DNAH9 (amino acids 3540–3839), using lipofectamine 3000 (Invitrogen, L3000015). 24 h later, immunoblotting and IF staining were performed. Sequences of primers used are: for 3xFlag-hDNAH17-C300, forward 5'-GATTACAAAGACGATGACGATAAAGAGGTGGAGTACCACCCCAAGT-3' and reverse 5'-GATCTAGAGTCGCGGCCGCTCTCCTTGGGGAAGATCTCCTTC-3'; for 3xFlag-mDNAH17-C300, forward 5'-GATTACAAAGACGATGACGATAAAGAGTACCACCCCAAGT-3' and reverse 5'-GATCTAGAGTCGCGGCCGCTCTCCTTGGGGAAGATCTCCTTC-3'; for 3xFlag-hDNAH11-C300, forward 5'-GATTACAAAGACGATGACGATAAAGAATGTGAATTTAACAAGAAC TTTC-3' and reverse 5'-GATCTAGAGTCGCGGCCGCTTCTTGA GGTAATTTTCTTTTCT-3'; for 3xFlag-mDNAH11-C300, forward 5'-GATTACAAAGACGATGACGATAAAGAATGCGAATTC AACAGAACTTCC-3' and reverse 5'-GATCTAGAGTCGCGGCCG CTTTCTTGGGTAAC TTTTCTTTTCA-3'; for 3xFlag-hDNAH9-C300, forward 5'-GATTACAAAGACGATGACGATAAATGTGAA TACAATCCCAAGTCCGGC-3' and reverse 5'-GATCTAGAGTCG CGGCCGCTCCACTCCTGTGGGAGCTTCTTTC-3'; and for 3xFlag-mDNAH9-C300, forward 5'-GATTACAAAGACGATGACGATAAAGAGTGTGAATTC AATCCCAAGTCC-3' and reverse 5'-GATCTAGAGTCGCGGCCGCTCTCCTGGGGAAGTCTCCTTC TCG-3'.

Immunoblotting

The HepG2 (ATCC, HB-8065), HEK293T, HCT116 (ATCC, CCL-247), A549 (ATCC, CCL-185), U-2 OS (ATCC, HTB-96), and HeLa (ATCC, CCL-2) cells were cultured in high-glucose DMEM (HyClone, SH30022.01) supplemented with 10% FBS (GIBCO, 15140122), 100 U/ml penicillin, and 100 mg/ml streptomycin (GIBCO, 16000044). All the cultures were maintained at 5% CO₂ at 37°C. For immunoblotting with cell lysates, cultured cells were washed with ice-cold PBS, lysed in 4X Bolt LDS Sample Buffer (Invitrogen, B0008) with NuPAGE Antioxidant (Invitrogen, NP0005), and boiled for 10 min. The cell lysates were subsequently stored at -80°C until use. Protein extracts from testes or spermatozoa from cauda epididymis were prepared using lysis buffer (50 mM Tris, pH 7.5, 150 mM NaCl, 0.5% Triton X-100, and 5 mM EDTA) containing a 1× PMSF protease inhibitor mixture (Thermo Scientific, 36978).

The proteins were then separated on a NuPAGE 3–8% Tris-Acetate Protein Gel (Invitrogen, EA03785BOX) and transferred to 0.45-μm pore-size nitrocellulose blotting membranes (GE Healthcare, 10600002) using a Mini Gel Tank (Invitrogen, A25977) electrophoresis and blotting apparatus (Tanon). Membranes were blocked with TBST buffer (50 mM Tris, pH 7.4, 150 mM NaCl, and 0.5% Tween-20) containing 5% nonfat milk for 1 h and incubated with primary antibodies diluted in TBST buffer containing 5% nonfat milk at 4°C overnight. Following incubation with secondary antibodies for 1 h, the blots were developed with chemiluminescence (ImageQuant LAS 4000, GE Healthcare). The primary antibodies that were used are mouse anti-α-tubulin (Sigma, F2168; 1:2,000), rabbit anti-Lamin B1 (Proteintech, 12987-1-AP; 1:2,000), mouse anti-GAPDH

(Proteintech, 60004-1-Ig; 1:3,000), rabbit anti-β-actin (Abcam, ab8227; 1:2,000), rabbit anti-β-tubulin (Abcam, ab6046; 1:3,000), rabbit anti-ODF2 (Proteintech, 12058-1-AP; 1:1,000), and the rabbit anti-DNAH17 antibody that was custom produced by ABclonal Biotechnology. The secondary antibodies that were used are HRP-conjugated donkey anti-rabbit IgG (Biolegend, 406401; 1:10,000) and HRP-conjugated goat anti-mouse IgG (Biolegend, 405306; 1:10,000).

IF staining

Human respiratory epithelial cells were obtained from a healthy subject by transnasal brush biopsy using disposable cytology brushes (Olympus, BC-202D-3010) and then spread onto glass slides. Mouse respiratory epithelial cells were obtained from tracheal tissues. The tracheae were cut into pieces gently, followed by centrifugation. After discarding the supernatant, the cells were resuspended in PBS containing 50% FBS and then spread onto glass slides. Human semen smears were prepared following the guideline of WHO (WHO, 2010). Mouse sperm were obtained from cauda epididymides, washed in PBS twice, and spread onto glass slides. The slides were air dried, fixed with 4% paraformaldehyde, and stored at -80°C until use.

For IF staining, slides were permeabilized with 0.1% (for sperm) or 0.2% Triton X-100 (for respiratory cells) in PBS and blocked with 3% skim milk. They were incubated with primary antibodies at 4°C overnight, followed by secondary antibodies at 37°C for 1 h, and then mounted with VECTASHIELD mounting medium (Vector Laboratories, H-1000) along with Hoechst 33342 (Invitrogen, H21492). Images of spermatozoa were captured using a Nikon ECLIPSE 80i microscope equipped with a charge-coupled device (Hamamatsu). Images of respiratory cilia were captured using the Nikon C2 Plus Confocal Laser Scanning Microscope system. The antibodies used were anti-α-tubulin (Sigma, F2168; 1:200), rabbit control IgG (Abclonal, AC005; 1:100), Alexa Fluor 488 goat anti-mouse IgG (Molecular Probes, A-21121; 1:100), and Alexa Fluor 555 donkey anti-rabbit IgG (Molecular Probes, A31572; 1:200). The customized anti-DNAH17 antibody was produced by ABclonal Biotechnology.

Immunohistochemistry and histological analyses of testicular and/or epididymal tissues

Fresh testicular and epididymal tissues were fixed in Bouin's solution or in 4% paraformaldehyde at 4°C overnight, followed by paraffin embedding. Paraffin-embedded tissues were sectioned (5 μm). Immunohistochemistry and IF staining of testicular sections were performed as previously described (Jiang et al., 2015; Jiang et al., 2014). The antibodies used were normal rabbit IgG (CST, 2729S; 1:100), Alexa Fluor 555 donkey anti-rabbit IgG (Molecular Probes, A31572; 1:200), and the anti-DNAH17 antibody that was custom produced by ABclonal Biotechnology. H&E and periodic acid-Schiff staining were performed for histological analyses of epididymal and testicular sections, respectively. Images were captured using a microscope (Nikon Eclipse 80i) equipped with a digital camera (Nikon DS-R1i).

TEM analysis

TEM was performed as previously described, with minor modifications (Yuan et al., 2015). Briefly, spermatozoa or tissues were fixed in 0.1 M phosphate buffer (PB; pH 7.4) containing 4% paraformaldehyde, 8% glutaraldehyde, and 0.2% picric acid at 4°C for at least overnight. After four washes with 0.1 M PB, samples were post-fixed with 1% OsO₄ and dehydrated, followed by infiltration of acetone and epon resin mixture. Samples were embedded and ultrathin (70 nm) sectioned before staining with uranyl acetate and lead citrate. The ultrastructure of the samples was examined and captured by Tecnai 10 or 12 Microscope (Philips) at 100 kV or 120 kV, or by H-7650 Microscope (Hitachi) at 100 kV.

Mouse models

Dnah17^{-/-} mice and *Dnah17*^{M/M} mice were generated by CRISPR/Cas9-mediated genome editing (Yang et al., 2013). Briefly, guide RNAs (gRNAs), targeting exon 3 (gRNA1 and gRNA2) for generating *Dnah17* knockouts or targeting exon 35 (gRNA3) for generating *Dnah17*^{M/M} mice, were transcribed in vitro (Addgene, 51132). Single-strand oligodeoxynucleotides (ssODNs), with a mutation equivalent to that in patients and a synonymous mutation at the protospacer adjacent motif, was synthesized by Sangon Biotech. The gRNA1/gRNA2 or ssODNs/gRNA3 were microinjected together with Cas9 mRNAs into zygotes of B6D2F1 (C57BL/6×DBA/2J) mice (Shen et al., 2014). Genotypes of the resulting pups were determined by Sanger sequencing. The founder mice, homozygous for a missense mutation in *Dnah17* (*Dnah17*^{M/M}) or heterozygous for *Dnah17* knockout (*Dnah17*^{+/-}), were backcrossed onto C57BL/6 background for at least two generations, and the resulting *Dnah17*^{+M} or *Dnah17*^{+/-} mice were crossed to generate *Dnah17*^{M/M} or *Dnah17*^{-/-} mice for our experiments. All mouse experiments were approved by the institutional animal ethics committee at the University of Science and Technology of China. The sequences of gRNAs, ssODNs, and genotyping primers are as follows: for gRNA1, 5'-TCGAGACCA TCATCATCGAC-3'; for gRNA2, 5'-GCCCGGGTGGAAATTTGA GT-3'; for gRNA3, 5'-ACATCTGTGACGCTCAGATC-3'; for ssODNs, 5'-CTTCACCTGGCAGTCGCAGCTTCGACACCGCTGGGA CGAGGAAAAGAAGCACTGCTTCGCAAACATCTATGACGCTCA GATCAAATACTCTACGAGTACCTGGGCAACACACCTCGGCT GGTCATCAC-3'; for *Dnah17*^{-/-} mouse genotyping, forward 5'-ACAAGAGCATCATCCGAC-3' and reverse 5'-GATTGGGTATC TGGCTCA-3'; and for *Dnah17*^{M/M} mouse genotyping, forward 5'-TGGAAGCCCTATCTGTAGC-3' and reverse 5'-TCCGGGAAC TAAATGGTCAAA-3'.

Fertility test

A fertility test was performed by mating one 10-wk-old *Dnah17*^{M/M} male with two 10-wk-old WT female mice (C57BL/6J) for 90 d. A total of five *Dnah17*^{M/M}, three *Dnah17*^{+M}, and three WT male mice were tested. All the females were monitored for pregnancy. Dates of birth and numbers of pups were recorded for all the litters.

Analyses of mouse sperm count, morphology, and motility

10-wk-old mice were sacrificed by cervical dislocation. Sperm number and motility were analyzed as previously described

(Castaneda et al., 2017; Jiang et al., 2017). For sperm morphology, slides were stained by Papanicolaou staining (Solarbio, G1612) according to the manufacturer's protocol. The percentages of morphologically normal spermatozoa were quantified according to the WHO guidelines (WHO, 2010), with at least 500 spermatozoa examined for each mouse.

Epididymal duct ligation

Adult mice were anaesthetized by intraperitoneal administration of tribromoethanol. The epididymides of both sides were exposed through a median incision at the lower abdomen and ligated with a surgical suture at the end of the corpus adjacent to cauda. The mice were euthanized 2 or 4 d after the operation. The epididymides were removed, with one side fixed in Bouin's for histological analyses by H&E staining and the other side fixed in 0.1 M PB containing 4% paraformaldehyde, 8% glutaraldehyde, and 0.2% picric acid for TEM analyses.

Online supplemental material

Fig. S1 presents WES data analysis. In Fig. S2, the alignment of human and mouse DNAH17 protein sequences show that 91% of amino acids are identical. Fig. S3 presents validation of the anti-DNAH17 antibody in transfected cells and *Dnah17* knockout mice. Fig. S4 shows morphological and axoneme ultrastructural analyses of spermatozoa from patients. Fig. S5 shows generation of *Dnah17*^{M/M} mice modeling patients' mutation and histological examinations of testes and epididymides from *Dnah17*^{+/+}, *Dnah17*^{+M}, and *Dnah17*^{M/M} mice.

Acknowledgments

We are grateful to all the participants for their cooperation. We thank Li Wang at the Center of Cryo-Electron Microscopy, Zhejiang University, for her technical assistance on TEM and the Al-Khair Test Lab, Abbottabad, Pakistan, for providing facilities to perform semen analysis. We thank Dr. Qing Wei (Shanghai Institutes for Biological Sciences) for his valuable suggestions and Dr. Fang Wang, Dr. Manan Khan Jadoon, and other members of the Q. Shi laboratory for comments and advice.

This work was supported by National Key Research and Developmental Program of China grants 2016YFC1000600, 2018YFC1004700, and 2018YFC1003900, Strategic Priority Research Program of the Chinese Academy of Sciences grant XDB19000000, National Natural Science Foundation of China grants 31890780, 31630050, 31771668, 31871514, 31601160, and 81571495, Major Program of Development Foundation of Hefei Centre for Physical Science and Technology grant 2018ZYFX005, and Fundamental Research Funds for the Central Universities grants YD2070003006, WK207000135, and WK207000136.

The authors declare no competing financial interests.

Author contributions: B. Zhang, T. Li, A. Ma, Y. Li, C. Yu, H. Yin, Q. Gao, X. Jiang, Q. Tao, Q. Hao, H. Fang, and H. Cheng performed the experiments; T. Khan, A. Ali, G. Murtaza, I. Khan, M. Zubair, H.M.J. Hussain, R. Khan, and A. Yousaf recruited the patients, performed semen analysis, and collected patient samples; J. Bao, F. Zhang, and C. Liu gave insightful discussion and

constructive comments on the manuscript; L. Yuan and Y. Lu provided technique assistance for TEM analysis; X. Xu and Y. Wang provided assistance for experiments with human respiratory epithelial cells; H. Zhang, J. Gao, and J. Zhou performed the WES sequencing and WES data analysis. Q. Shi, H. Ma, and Y. Zhang conceived and supervised the study, designed and analyzed experiments, and wrote the manuscript.

Submitted: 20 December 2018

Revised: 10 June 2019

Accepted: 3 October 2019

References

- Adams, J.A., T.S. Galloway, D. Mondal, S.C. Esteves, and F. Mathews. 2014. Effect of mobile telephones on sperm quality: a systematic review and meta-analysis. *Environ. Int.* 70:106–112. <https://doi.org/10.1016/j.envint.2014.04.015>
- Adzhubei, I.A., S. Schmidt, L. Peshkin, V.E. Ramensky, A. Gerasimova, P. Bork, A.S. Kondrashov, and S.R. Sunyaev. 2010. A method and server for predicting damaging missense mutations. *Nat. Methods.* 7:248–249. <https://doi.org/10.1038/nmeth0410-248>
- Amos, L., and A. Klug. 1974. Arrangement of subunits in flagellar microtubules. *J. Cell Sci.* 14:523–549.
- Auton, A., L.D. Brooks, R.M. Durbin, E.P. Garrison, H.M. Kang, J.O. Korbel, J.L. Marchini, S. McCarthy, G.A. McVean, and G.R. Abecasis. 1000 Genomes Project Consortium. 2015. A global reference for human genetic variation. *Nature.* 526:68–74. <https://doi.org/10.1038/nature15393>
- Bartoloni, L., J.-L. Blouin, Y. Pan, C. Gehrig, A.K. Maiti, N. Scamuffa, C. Rossier, M. Jorissen, M. Armengot, M. Meeks, et al. 2002. Mutations in the DNAH11 (axonemal heavy chain dynein type 11) gene cause one form of situs inversus totalis and most likely primary ciliary dyskinesia. *Proc. Natl. Acad. Sci. USA.* 99:10282–10286. <https://doi.org/10.1073/pnas.152337699>
- Ben Khelifa, M., C. Coutton, R. Zouari, T. Karaouzen, J. Rendu, M. Bidart, S. Yassine, V. Pierre, J. Delaroche, S. Hennebicq, et al. 2014. Mutations in DNAH1, which encodes an inner arm heavy chain dynein, lead to male infertility from multiple morphological abnormalities of the sperm flagella. *Am. J. Hum. Genet.* 94:95–104. <https://doi.org/10.1016/j.ajhg.2013.11.017>
- Castaneda, J.M., R. Hua, H. Miyata, A. Oji, Y. Guo, Y. Cheng, T. Zhou, X. Guo, Y. Cui, B. Shen, et al. 2017. TCTE1 is a conserved component of the dynein regulatory complex and is required for motility and metabolism in mouse spermatozoa. *Proc. Natl. Acad. Sci. USA.* 114:E5370–E5378. <https://doi.org/10.1073/pnas.1621279114>
- Choi, Y., G.E. Sims, S. Murphy, J.R. Miller, and A.P. Chan. 2012. Predicting the functional effect of amino acid substitutions and indels. *PLoS One.* 7: e46688. <https://doi.org/10.1371/journal.pone.0046688>
- Chun, S., and J.C. Fay. 2009. Identification of deleterious mutations within three human genomes. *Genome Res.* 19:1553–1561. <https://doi.org/10.1101/gr.092619.109>
- Coutton, C., A.S. Vargas, A. Amiri-Yekta, Z.-E. Kherraf, S.F. Ben Mustapha, P. Le Tanno, C. Wambergue-Legendre, T. Karaouzen, G. Martinez, S. Crouzy, et al. 2018. Mutations in CFAP43 and CFAP44 cause male infertility and flagellum defects in Trypanosoma and human. *Nat. Commun.* 9:686. <https://doi.org/10.1038/s41467-017-02792-7>
- Curi, S.M., J.I. Ariagno, P.H. Chenlo, G.R. Mendeluk, M.N. Pugliese, L.M. Sardi Segovia, H.E. Repetto, and A.M. Blanco. 2003. Asthenozoospermia: analysis of a large population. *Arch. Androl.* 49:343–349. <https://doi.org/10.1080/01485010390219656>
- Dacheux, J.-L., and F. Dacheux. 2013. New insights into epididymal function in relation to sperm maturation. *Reproduction.* 147:R27–R42. <https://doi.org/10.1530/REP-13-0420>
- Davydov, E.V., D.L. Goode, M. Sirota, G.M. Cooper, A. Sidow, and S. Batzoglou. 2010. Identifying a high fraction of the human genome to be under selective constraint using GERP++. *PLOS Comput. Biol.* 6:e1001025. <https://doi.org/10.1371/journal.pcbi.1001025>
- Dong, C., P. Wei, X. Jian, R. Gibbs, E. Boerwinkle, K. Wang, and X. Liu. 2015. Comparison and integration of deleteriousness prediction methods for nonsynonymous SNVs in whole exome sequencing studies. *Hum. Mol. Genet.* 24:2125–2137. <https://doi.org/10.1093/hmg/ddu733>
- Dougherty, G.W., N.T. Loges, J.A. Klinckenbusch, H. Olbrich, P. Pennekamp, T. Menchen, J. Raidt, J. Wallmeier, C. Werner, C. Westermann, et al. 2016. DNAH11 localization in the proximal region of respiratory cilia defines distinct outer dynein arm complexes. *Am. J. Respir. Cell Mol. Biol.* 55: 213–224. <https://doi.org/10.1165/rcmb.2015-0353OC>
- Fassad, M.R., A. Shoemark, M. Legendre, R.A. Hirst, F. Koll, P. le Borgne, B. Louis, F. Daudvohra, M.P. Patel, L. Thomas, et al. 2018. Mutations in outer dynein arm heavy chain DNAH9 cause motile cilia defects and situs inversus. *Am. J. Hum. Genet.* 103:984–994. <https://doi.org/10.1016/j.ajhg.2018.10.016>
- Fliegau, M., H. Olbrich, J. Horvath, J.H. Wildhaber, M.A. Zariwala, M. Kennedy, M.R. Knowles, and H. Omran. 2005. Mislocalization of DNAH5 and DNAH9 in respiratory cells from patients with primary ciliary dyskinesia. *Am. J. Respir. Crit. Care Med.* 171:1343–1349. <https://doi.org/10.1164/rccm.200411-1583OC>
- Fu, W., T.D. O'Connor, G. Jun, H.M. Kang, G. Abecasis, S.M. Leal, S. Gabriel, M.J. Rieder, D. Altshuler, J. Shendure, et al. NHLBI Exome Sequencing Project. 2013. Analysis of 6,515 exomes reveals the recent origin of most human protein-coding variants. *Nature.* 493:216–220. <https://doi.org/10.1038/nature11690>
- Gibbons, I.R. 1963. Studies on the protein components of cilia from Tetrahymena pyriformis. *Proc. Natl. Acad. Sci. USA.* 50:1002–1010. <https://doi.org/10.1073/pnas.50.5.1002>
- Hornef, N., H. Olbrich, J. Horvath, M.A. Zariwala, M. Fliegau, N.T. Loges, J. Wildhaber, P.G. Noone, M. Kennedy, S.E. Antonarakis, et al. 2006. DNAH5 mutations are a common cause of primary ciliary dyskinesia with outer dynein arm defects. *Am. J. Respir. Crit. Care Med.* 174:120–126. <https://doi.org/10.1164/rccm.200601-084OC>
- Inaba, K. 2011. Sperm flagella: comparative and phylogenetic perspectives of protein components. *Mol. Hum. Reprod.* 17:524–538. <https://doi.org/10.1093/molehr/gar034>
- Ji, Z.-Y., Y.W. Sha, L. Ding, and P. Li. 2017. Genetic factors contributing to human primary ciliary dyskinesia and male infertility. *Asian J. Androl.* 19:515–520. <https://doi.org/10.4103/1008-682X.181227>
- Jiang, X., H. Zhang, S. Yin, Y. Zhang, W. Yang, W. Zheng, L. Wang, Z. Wang, I. Bukhari, H.J. Cooke, et al. 2014. Specific deficiency of Plzf paralog, Zbtb20, in Sertoli cells does not affect spermatogenesis and fertility in mice. *Sci. Rep.* 4:7062. <https://doi.org/10.1038/srep07062>
- Jiang, X., T. Ma, Y. Zhang, H. Zhang, S. Yin, W. Zheng, L. Wang, Z. Wang, M. Khan, S.W. Sheikh, et al. 2015. Specific deletion of Cdh2 in Sertoli cells leads to altered meiotic progression and subfertility of mice. *Biol. Reprod.* 92:1–12. <https://doi.org/10.1095/biolreprod.114.126334>
- Jiang, L., T. Li, X. Zhang, B. Zhang, C. Yu, Y. Li, S. Fan, X. Jiang, T. Khan, Q. Hao, et al. 2017. RPL10L is required for male meiotic division by compensating for RPL10 during meiotic sex chromosome inactivation in mice. *Curr. Biol.* 27:1498–1505.e6. <https://doi.org/10.1016/j.cub.2017.04.017>
- Kikkawa, M. 2013. Big steps toward understanding dynein. *J. Cell Biol.* 202: 15–23. <https://doi.org/10.1083/jcb.201304099>
- Knowles, M.R., M.W. Leigh, J.L. Carson, S.D. Davis, S.D. Dell, T.W. Ferkol, K.N. Olivier, S.D. Sagel, M. Rosenfeld, K.A. Burns, et al. Genetic Disorders of Mucociliary Clearance Consortium. 2012. Mutations of DNAH11 in patients with primary ciliary dyskinesia with normal ciliary ultrastructure. *Thorax.* 67:433–441. <https://doi.org/10.1136/thoraxjnl-2011-200301>
- Konno, A., K. Ikegami, Y. Konishi, H.-J. Yang, M. Abe, M. Yamazaki, K. Sakimura, I. Yao, K. Shiba, K. Inaba, and M. Setou. 2016. Ttl9-/- mice sperm flagella show shortening of doublet 7, reduction of doublet 5 polyglutamylation and a stall in beating. *J. Cell Sci.* 129:2757–2766. <https://doi.org/10.1242/jcs.185983>
- Leigh, M.W., J.E. Pittman, J.L. Carson, T.W. Ferkol, S.D. Dell, S.D. Davis, M.R. Knowles, and M.A. Zariwala. 2009. Clinical and genetic aspects of primary ciliary dyskinesia/Kartagener syndrome. *Genet. Med.* 11: 473–487. <https://doi.org/10.1097/GIM.0b013e3181a53562>
- Lek, M., K.J. Karczewski, E.V. Minikel, K.E. Samocha, E. Banks, T. Fennell, A.H. O'Donnell-Luria, J.S. Ware, A.J. Hill, B.B. Cummings, et al. Exome Aggregation Consortium. 2016. Analysis of protein-coding genetic variation in 60,706 humans. *Nature.* 536:285–291. <https://doi.org/10.1038/nature19057>
- Li, Y., H. Yagi, E.O. Onuoha, R.R. Damerla, R. Francis, Y. Furutani, M. Tariq, S.M. King, G. Hendricks, C. Cui, et al. 2016. DNAH6 and its interactions with PC2 genes in heterotaxy and primary ciliary dyskinesia. *PLoS Genet.* 12:e1005821. <https://doi.org/10.1371/journal.pgen.1005821>
- Lindblad-Toh, K., M. Garber, O. Zuk, M.F. Lin, B.J. Parker, S. Washietl, P. Kheradpour, J. Ernst, G. Jordan, E. Mauceli, et al. Genome Institute at

- Washington University. 2011. A high-resolution map of human evolutionary constraint using 29 mammals. *Nature*. 478:476–482. <https://doi.org/10.1038/nature10530>
- Loges, N.T., D. Antony, A. Maver, M.A. Deardorff, E.Y. Güleç, A. Gezirici, T. Nöthe-Menchen, I.M. Höben, L. Jelten, D. Frank, et al. 2018. Recessive DNAH9 Loss-of-Function Mutations Cause Laterality Defects and Subtle Respiratory Ciliary-Beating Defects. *Am. J. Hum. Genet.* 103:995–1008. <https://doi.org/10.1016/j.ajhg.2018.10.020>
- Lucas, J.S., E.C. Adam, P.M. Goggin, C.L. Jackson, N. Powles-Glover, S.H. Patel, J. Humphreys, M.D. Fray, E. Falconnet, J.L. Blouin, et al. 2012. Static respiratory cilia associated with mutations in Dnahc11/DNAH11: a mouse model of PCD. *Hum. Mutat.* 33:495–503. <https://doi.org/10.1002/humu.22001>
- Martinez, G., Z.-E. Kherraf, R. Zouari, S. Fourati Ben Mustapha, A. Saut, K. Pernet-Gallay, A. Bertrand, M. Bidart, J.P. Hograindeur, A. Amir-Yekta, et al. 2018. Whole-exome sequencing identifies mutations in FSP2 as a recurrent cause of multiple morphological abnormalities of the sperm flagella. *Hum. Reprod.* 33:1973–1984. <https://doi.org/10.1093/humrep/dey264>
- Milisav, I., and N.A. Affara. 1998. A potential human axonemal dynein heavy-chain gene maps to 17q25. *Mamm. Genome*. 9:404–407. <https://doi.org/10.1007/s003359900782>
- Neesen, J., R. Kirschner, M. Ochs, A. Schmiedl, B. Habermann, C. Mueller, A.F. Holstein, T. Nuesslein, I. Adham, and W. Engel. 2001. Disruption of an inner arm dynein heavy chain gene results in asthenozoospermia and reduced ciliary beat frequency. *Hum. Mol. Genet.* 10:1117–1128. <https://doi.org/10.1093/hmg/10.11.1117>
- Olbrich, H., K. Häffner, A. Kispert, A. Völkel, A. Volz, G. Sasmaz, R. Reinhardt, S. Hennig, H. Lehrach, N. Konietzko, et al. 2002. Mutations in DNAH5 cause primary ciliary dyskinesia and randomization of left-right asymmetry. *Nat. Genet.* 30:143–144. <https://doi.org/10.1038/ng817>
- Ortega, C., G. Verheyen, D. Raick, M. Camus, P. Devroey, and H. Tournaye. 2011. Absolute asthenozoospermia and ICSI: what are the options? *Hum. Reprod. Update*. 17:684–692. <https://doi.org/10.1093/humupd/dmr018>
- Pazour, G.J., N. Agrin, B.L. Walker, and G.B. Witman. 2006. Identification of predicted human outer dynein arm genes: candidates for primary ciliary dyskinesia genes. *J. Med. Genet.* 43:62–73. <https://doi.org/10.1136/jmg.2005.033001>
- Pifferi, M., A. Michelucci, M.E. Conidi, A.M. Cangiotti, P. Simi, P. Macchia, and A.L. Boner. 2010. New DNAH11 mutations in primary ciliary dyskinesia with normal axonemal ultrastructure. *Eur. Respir. J.* 35:1413–1416. <https://doi.org/10.1183/09031936.00186209>
- Reva, B., Y. Antipin, and C. Sander. 2011. Predicting the functional impact of protein mutations: application to cancer genomics. *Nucleic Acids Res.* 39:e118. <https://doi.org/10.1093/nar/gkr407>
- Richards, S., N. Aziz, S. Bale, D. Bick, S. Das, J. Gastier-Foster, W.W. Grody, M. Hegde, E. Lyon, E. Spector, et al. ACMG Laboratory Quality Assurance Committee. 2015. Standards and guidelines for the interpretation of sequence variants: a joint consensus recommendation of the American College of Medical Genetics and Genomics and the Association for Molecular Pathology. *Genet. Med.* 17:405–424. <https://doi.org/10.1038/gim.2015.30>
- Roberts, A.J., T. Kon, P.J. Knight, K. Sutoh, and S.A. Burgess. 2013. Functions and mechanics of dynein motor proteins. *Nat. Rev. Mol. Cell Biol.* 14:713–726. <https://doi.org/10.1038/nrm3667>
- Salas-Huetos, A., M. Bulló, and J. Salas-Salvadó. 2017. Dietary patterns, foods and nutrients in male fertility parameters and fecundability: a systematic review of observational studies. *Hum. Reprod. Update*. 23:371–389. <https://doi.org/10.1093/humupd/dmx006>
- Sampson, M.J., W.K. Decker, A.L. Beaudet, W. Ruitenbeek, D. Armstrong, M.J. Hicks, and W.J. Craigen. 2001. Immotile sperm and infertility in mice lacking mitochondrial voltage-dependent anion channel type 3. *J. Biol. Chem.* 276:39206–39212. <https://doi.org/10.1074/jbc.M104724200>
- Sato, H., Y. Taketomi, Y. Isogai, Y. Miki, K. Yamamoto, S. Masuda, T. Hosono, S. Arata, Y. Ishikawa, T. Ishii, et al. 2010. Group III secreted phospholipase A2 regulates epididymal sperm maturation and fertility in mice. *J. Clin. Invest.* 120:1400–1414. <https://doi.org/10.1172/JCI40493>
- Schwabe, G.C., K. Hoffmann, N.T. Loges, D. Birker, C. Rossier, M.M. de Santi, H. Olbrich, M. Fliegau, M. Faily, U. Liebers, et al. 2008. Primary ciliary dyskinesia associated with normal axoneme ultrastructure is caused by DNAH11 mutations. *Hum. Mutat.* 29:289–298. <https://doi.org/10.1002/humu.20656>
- Schwarz, J.M., D.N. Cooper, M. Schuelke, and D. Seelow. 2014. MutationTaster2: mutation prediction for the deep-sequencing age. *Nat. Methods*. 11:361–362. <https://doi.org/10.1038/nmeth.2890>
- Sha, Y., X. Yang, L. Mei, Z. Ji, X. Wang, L. Ding, P. Li, and S. Yang. 2017. DNAH1 gene mutations and their potential association with dysplasia of the sperm fibrous sheath and infertility in the Han Chinese population. *Fertil. Steril.* 107:1312–1318.e2. <https://doi.org/10.1016/j.fertnstert.2017.04.007>
- Shen, B., W. Zhang, J. Zhang, J. Zhou, J. Wang, L. Chen, L. Wang, A. Hodgkins, V. Iyer, X. Huang, and W.C. Skarnes. 2014. Efficient genome modification by CRISPR-Cas9 nickase with minimal off-target effects. *Nat. Methods*. 11:399–402. <https://doi.org/10.1038/nmeth.2857>
- Shihab, H.A., J. Gough, D.N. Cooper, P.D. Stenson, G.L. Barker, K.J. Edwards, I.N. Day, and T.R. Gaunt. 2013. Predicting the functional, molecular, and phenotypic consequences of amino acid substitutions using hidden Markov models. *Hum. Mutat.* 34:57–65. <https://doi.org/10.1002/humu.22225>
- Shihab, H.A., M.F. Rogers, J. Gough, M. Mort, D.N. Cooper, I.N. Day, T.R. Gaunt, and C. Campbell. 2015. An integrative approach to predicting the functional effects of non-coding and coding sequence variation. *Bioinformatics*. 31:1536–1543. <https://doi.org/10.1093/bioinformatics/btv009>
- Shum, W.W., N. Da Silva, D. Brown, and S. Breton. 2009. Regulation of luminal acidification in the male reproductive tract via cell-cell crosstalk. *J. Exp. Biol.* 212:1753–1761. <https://doi.org/10.1242/jeb.027284>
- Sim, N.-L., P. Kumar, J. Hu, S. Henikoff, G. Schneider, and P.C. Ng. 2012. SIFT web server: predicting effects of amino acid substitutions on proteins. *Nucleic Acids Res.* 40:W452–W457. <https://doi.org/10.1093/nar/gks539>
- Smith, K.R., C.J. Bromhead, M.S. Hildebrand, A.E. Shearer, P.J. Lockhart, H. Najmabadi, R.J. Leventer, G. McGillivray, D.J. Amor, R.J. Smith, and M. Bahlo. 2011. Reducing the exome search space for mendelian diseases using genetic linkage analysis of exome genotypes. *Genome Biol.* 12:R85. <https://doi.org/10.1186/gb-2011-12-9-r85>
- Summers, K.E., and I.R. Gibbons. 1971. Adenosine triphosphate-induced sliding of tubules in trypsin-treated flagella of sea-urchin sperm. *Proc. Natl. Acad. Sci. USA*. 68:3092–3096. <https://doi.org/10.1073/pnas.68.12.3092>
- Tang, S., X. Wang, W. Li, X. Yang, Z. Li, W. Liu, C. Li, Z. Zhu, L. Wang, J. Wang, et al. 2017. Biallelic mutations in CFAP43 and CFAP44 cause male infertility with multiple morphological abnormalities of the sperm flagella. *Am. J. Hum. Genet.* 100:854–864. <https://doi.org/10.1016/j.ajhg.2017.04.012>
- Turner, T.T. 2008. De Graaf's thread: the human epididymis. *J. Androl.* 29:237–250. <https://doi.org/10.2164/jandrol.107.004119>
- Wang, X., H. Jin, F. Han, Y. Cui, J. Chen, C. Yang, P. Zhu, W. Wang, G. Jiao, W. Wang, et al. 2017. Homozygous DNAH1 frameshift mutation causes multiple morphological anomalies of the sperm flagella in Chinese. *Clin. Genet.* 91:313–321. <https://doi.org/10.1111/cge.12857>
- World Health Organization. 2010. *WHO Laboratory Manual for the Examination and Processing of Human Semen*. Fifth edition. World Health Organization, New York. 287 pp.
- Yang, H., H. Wang, C.S. Shivalila, A.W. Cheng, L. Shi, and R. Jaenisch. 2013. One-step generation of mice carrying reporter and conditional alleles by CRISPR/Cas-mediated genome engineering. *Cell*. 154:1370–1379. <https://doi.org/10.1016/j.cell.2013.08.022>
- Yin, H., H. Ma, S. Hussain, H. Zhang, X. Xie, L. Jiang, X. Jiang, F. Iqbal, I. Bukhari, H. Jiang, et al. 2019. A homozygous FANCM frameshift pathogenic variant causes male infertility. *Genet. Med.* 21:62–70. <https://doi.org/10.1038/s41436-018-0015-7>
- Yuan, S., C.J. Stratton, J. Bao, H. Zheng, B.P. Bhetwal, R. Yanagimachi, and W. Yan. 2015. Spata6 is required for normal assembly of the sperm connecting piece and tight head-tail conjunction. *Proc. Natl. Acad. Sci. USA*. 112:E430–E439. <https://doi.org/10.1073/pnas.1424648112>
- Zhang, Y., L. Zhong, B. Xu, Y. Yang, R. Ban, J. Zhu, H.J. Cooke, Q. Hao, and Q. Shi. 2013. SpermatogenesisOnline 1.0: a resource for spermatogenesis based on manual literature curation and genome-wide data mining. *Nucleic Acids Res.* 41(D1):D1055–D1062. <https://doi.org/10.1093/nar/gks1186>
- Zuccarello, D., A. Ferlin, C. Cazzadore, A. Pepe, A. Garolla, A. Moretti, G. Cordeschi, S. Francavilla, and C. Foresta. 2008. Mutations in dynein genes in patients affected by isolated non-syndromic asthenozoospermia. *Hum. Reprod.* 23:1957–1962. <https://doi.org/10.1093/humrep/den193>

Supplemental material

Zhang et al., <https://doi.org/10.1084/jem.20182365>

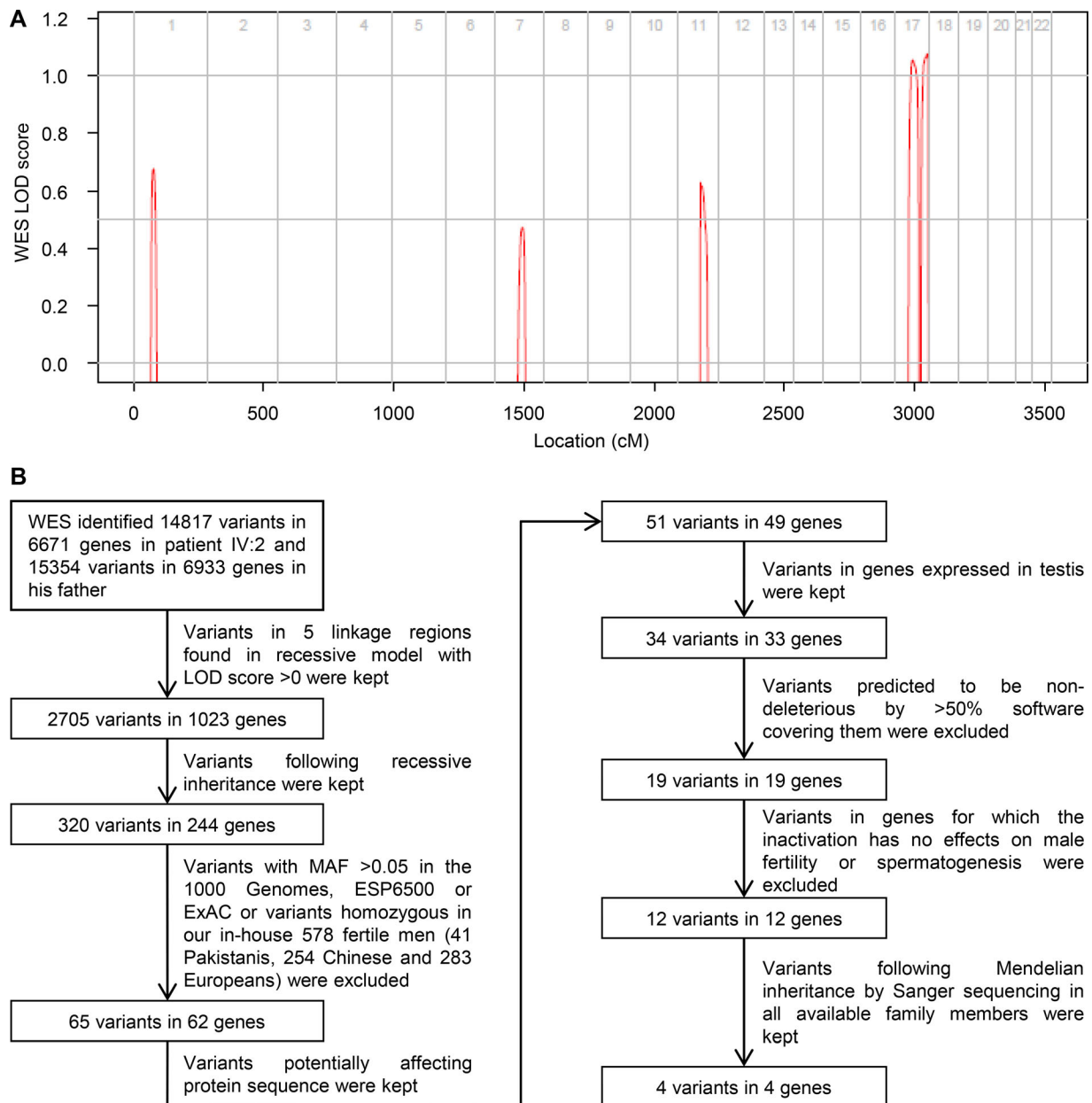


Figure S1. **WES data analysis.** (A) Genome-wide logarithm of the odds scores using WES-derived genotypes for the family. (B) WES data analysis pipeline. LOD, logarithm of the odds; MAF, minor allele frequency.

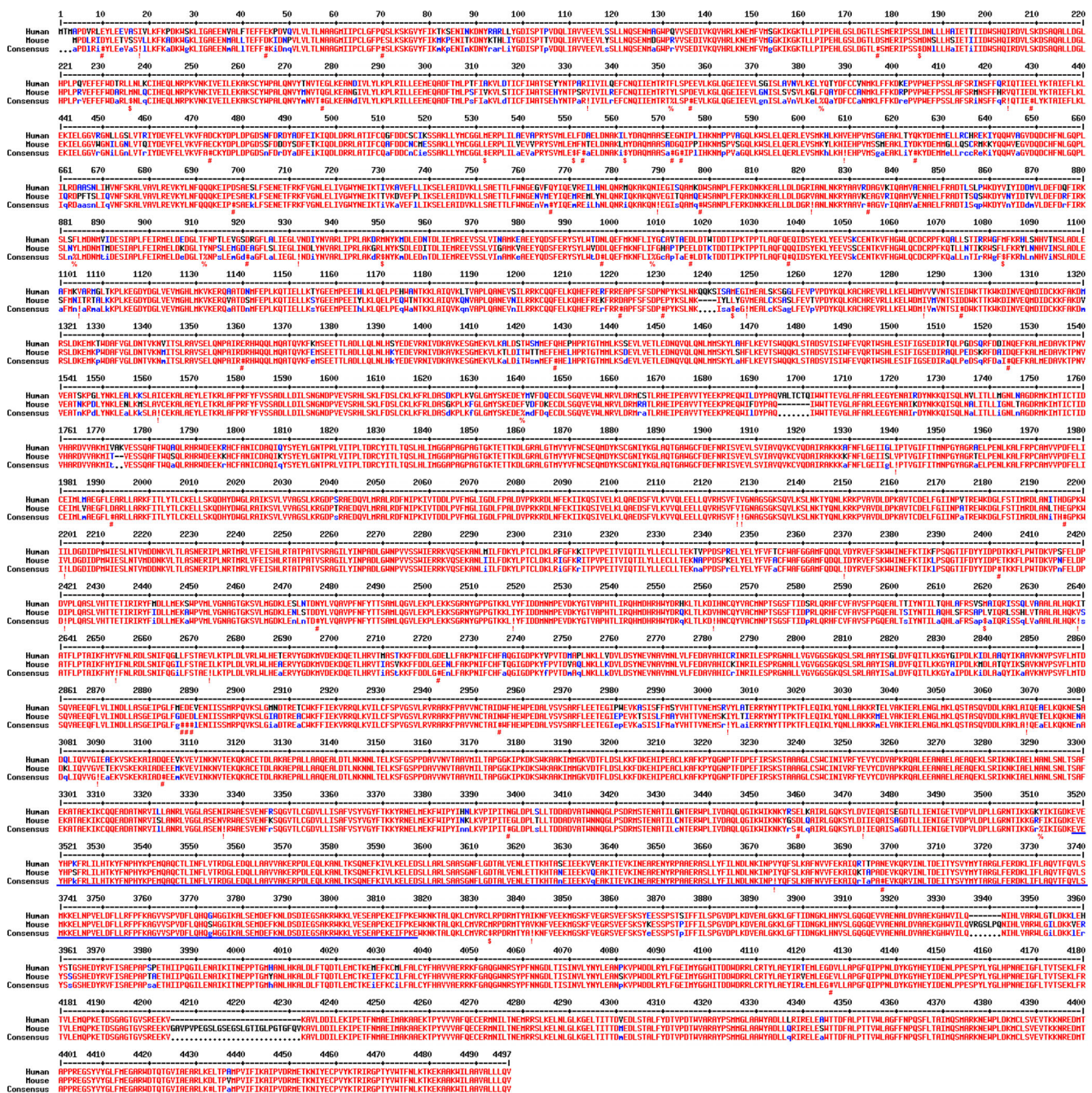


Figure S2. Alignment of human and mouse DNAH17 protein sequences showing that 91% of amino acids are identical. Residues that are identical between human and mouse DNAH17 appear in red and as uppercase letters in the consensus line. Residues highly similar between human and mouse DNAH17 are indicated by red symbols (I, any one of I and V; \$, any one of L and M; %, any one of F and Y; #, any one of N, D, Q, E, B, and Z). Unconserved residues are written in blue or as asterisks in the consensus line. Blue lines highlight the epitope (amino acids 3502–3801 for mouse DNAH17, corresponding to amino acids 3518–3817 in human DNAH17) for antibody generation. The alignment was performed using the online software MultAlin (<http://multalin.toulouse.inra.fr/multalin/multalin.html>).

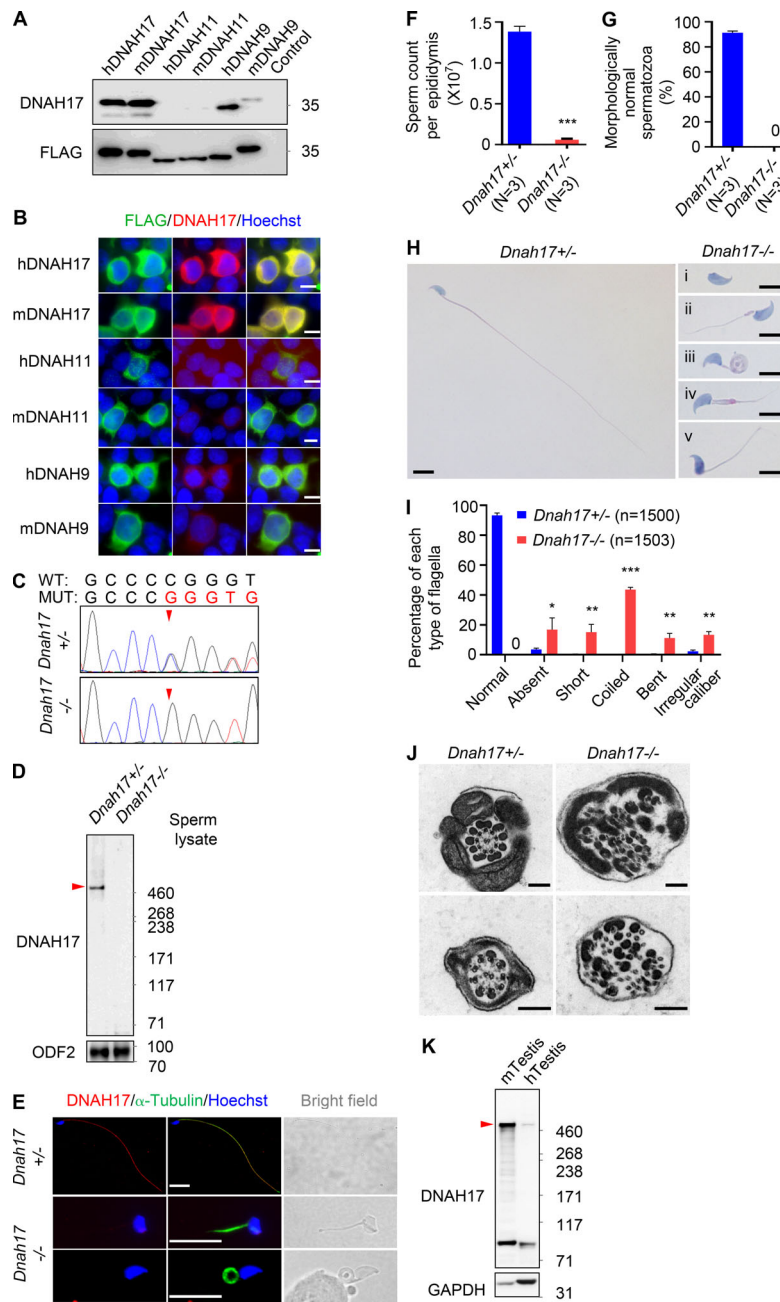


Figure S3. **Validation of the anti-DNAH17 antibody in transfected cells and *Dnah17* knockout mice.** (A and B) Immunoblotting (A) and IF staining (B) of HEK293T cells overexpressing the epitope-corresponding peptides from human DNAH17 (amino acids 3518–3817), mouse DNAH17 (amino acids 3502–3801), human DNAH11 (amino acids 3572–3871), mouse DNAH11 (amino acids 3544–3843), human DNAH9 (amino acids 3542–3841), or mouse DNAH9 (amino acids 3540–3839) with an N-terminal FLAG tag. For immunoblotting, untransfected cells were used as negative control. Two independent experiments were performed. Scale bars represent 10 μ m. (C) Genomic DNA sequencing chromatograms showing the one-nucleotide-deletion mutation (g.971_971del) in *Dnah17*^{-/-} mice. Arrowheads indicate the mutation site. WT, the wild-type allele. MUT, the mutant allele. (D) Immunoblotting using the anti-DNAH17 antibody detected a specific band at the predicted size of DNAH17 (512 kD), as indicated by the arrowhead, in spermatozoa from *Dnah17*^{+/-} mice, but not in spermatozoa from *Dnah17*^{-/-} mice. ODF2 (a marker of outer dense fibers) was used as the loading control. (E) Representative images of spermatozoa from *Dnah17*^{+/-} and *Dnah17*^{-/-} mice stained for DNAH17 and α -tubulin, a marker for sperm flagellum. Scale bars represent 10 μ m. (F) Sperm count per epididymis in *Dnah17*^{-/-} mice. (G) Quantification of the spermatozoa with normal morphology. (H) Representative images of spermatozoa after Papanicolaou staining showing absent (i), short (ii), coiled (iii), bent (iv), and irregular-caliber (v) flagella in *Dnah17*^{-/-} mice. Scale bars represent 5 μ m. (I) Frequencies of sperm flagella that were morphologically normal, absent, short, coiled, bent, or of irregular caliber. Each spermatozoon was classified as only one type of flagellar morphology according to its major abnormality. (J) Representative TEM micrographs showing cross sections of proximal (upper panel) and distal (lower panel) regions of sperm flagella from *Dnah17*^{+/-} and *Dnah17*^{-/-} mice. Scale bars represent 200 nm. (K) Immunoblotting using the anti-DNAH17 antibody detected a specific band of predicted size (510 kD for human DNAH17 and 512 kD for mouse DNAH17), as indicated by the arrowhead, in testicular lysates from adult WT mice (mTestis) or fertile men (hTestis). GAPDH was used as the loading control (GAPDH was predicted to be 35.8 kD in mouse and 36.1 kD in human). For A–K, at least two independent experiments were performed. (F, G, and I) Data are presented as mean \pm SEM. *P < 0.05, **P < 0.01, ***P < 0.001; Student’s *t* test. N, number of mice examined; n, number of spermatozoa examined.

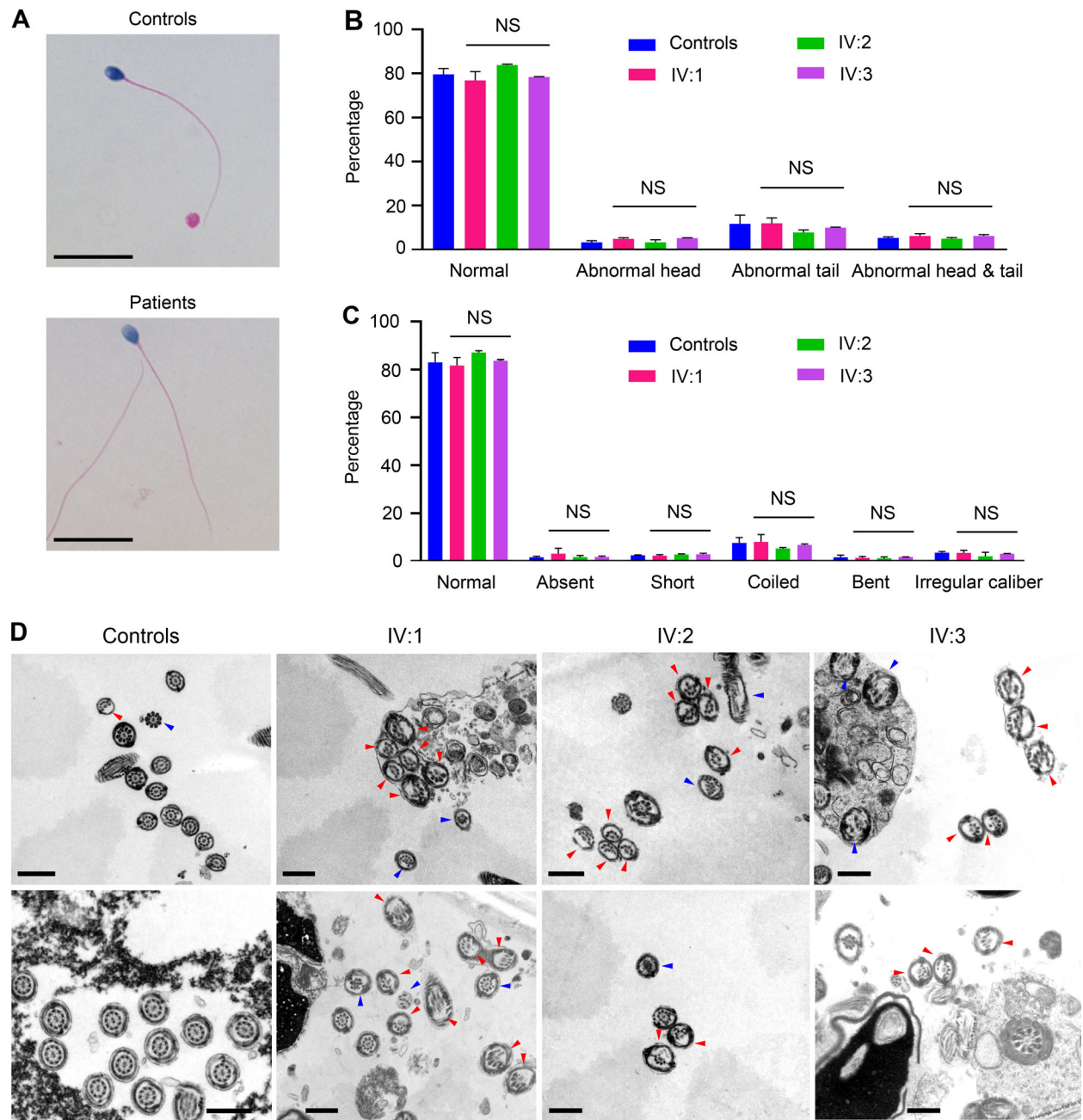


Figure S4. **Morphological and axoneme ultrastructural analyses of spermatozoa from patients.** (A) Representative images of spermatozoa from the fertile controls and patients after Papanicolaou staining. Scale bars represent 10 μ m. (B) Quantification of spermatozoa with normal morphology, or morphological defects in sperm head, tail, or head and tail. (C) Frequencies of sperm flagella that are morphologically normal, absent, short, coiled, bent, or of irregular caliber. Each spermatozoon was classified as only one type of flagellar morphology according to its major abnormality. For A and B, two independent experiments were performed with at least 500 spermatozoa examined per person each time. Data are presented as mean \pm SEM. Compared with the fertile control, one-way ANOVA with Dunnett's multiple comparison test. Two independent experiments were performed. (D) Representative TEM micrographs showing cross sections of sperm flagella at low magnification from fertile men (controls) and the three patients. Red arrowheads, cross sections with MTD(s) 4–7 missing; blue arrowheads, cross sections with abnormalities other than the loss of MTD(s) 4–7. Scale bars represent 500 nm.

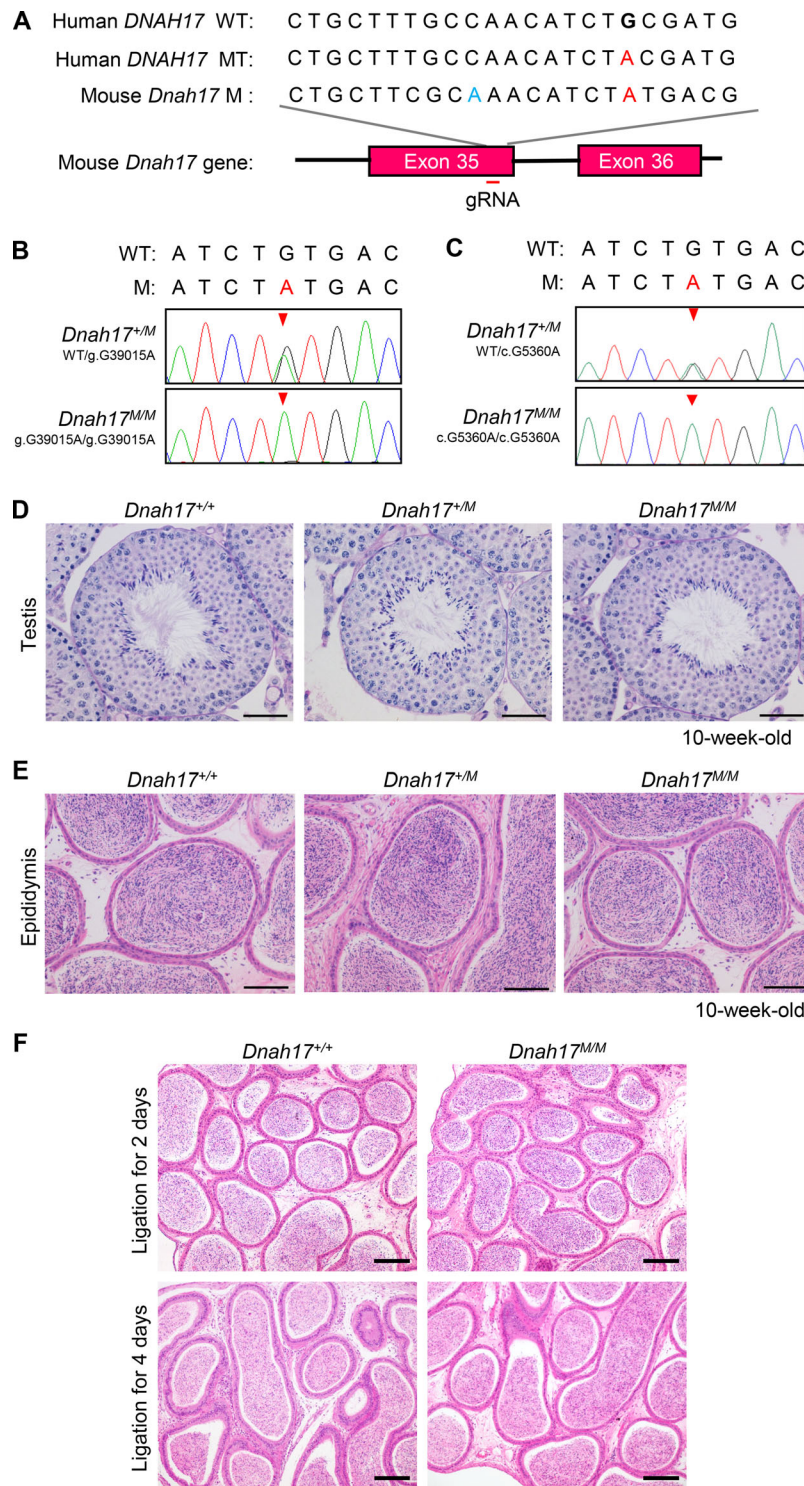


Figure S5. **Generation of *Dnah17*^{M/M} mice modeling patients' mutation and histological examinations of testes and epididymides from *Dnah17*^{+/+}, *Dnah17*^{+/M}, and *Dnah17*^{M/M} mice.** (A) Schematic illustrating construction of the mouse model (*Dnah17*^{M/M}). A gRNA was designed targeting exon 35 of *Dnah17*. The mutated nucleotides in mice (c.G5360A) and in patients (c.G5408A) are written in red. The nucleotide written in blue indicates a mutation not affecting the amino acid sequence in the protospacer adjacent motif, introduced by ssODNs. (B) Genomic DNA sequencing chromatograms showing the g.G39015A mutation heterozygous in *Dnah17*^{+/M} and homozygous in *Dnah17*^{M/M} mice. (C) cDNA sequencing chromatograms from *Dnah17*^{+/M} and *Dnah17*^{M/M} mice verified the c.G5360A mutation at mRNA level. (D) Periodic acid-Schiff staining of testicular sections showing that the spermatogenesis in *Dnah17*^{M/M} and *Dnah17*^{+/M} mice is comparable to that of *Dnah17*^{+/+} mice. Scale bars represent 50 μ m. (E) H&E staining of epididymal sections revealed similar sperm concentrations in *Dnah17*^{M/M} and *Dnah17*^{+/M} mice compared with that in *Dnah17*^{+/+} mice. Scale bars represent 100 μ m. (F) Histological examination of corpus epididymides from *Dnah17*^{+/+} and *Dnah17*^{M/M} mice after ligation for 2 d and 4 d. Two independent experiments were performed. Scale bars represent 100 μ m. (A-E) Three independent experiments were performed. Arrowheads, the mutation site; WT, the wild-type allele; MT, the mutant allele in humans; M, the mutant allele in mice.